Forschungszentrum Karlsruhe

in der Helmholtz-Gemeinschaft

Wissenschaftliche Berichte

FZKA 6817

Three-dimensional buoyant convection in a rectangular box with thin conducting walls in a strong horizontal magnetic field

S. Molokov[1] and L. Bühler

Institut für Kern- und Energietechnik
Programm Kernfusion

[1]Coventry University, School of Mathematical and Information Sciences, Priory Street, Coventry CV1 5FB, United Kingdom

Forschungszentrum Karlsruhe GmbH, Karlsruhe
2003

Impressum der Print-Ausgabe:

Als Manuskript gedruckt

Forschungszentrum Karlsruhe GmbH
Postfach 3640, 76021 Karlsruhe

Mitglied der Hermann von Helmholtz-Gemeinschaft
Deutscher Forschungszentren (HGF)

ISSN 0947-8620

Three-dimensional buoyant convection in a rectangular box with thin conducting walls in a strong horizontal magnetic field

Abstract

Three-dimensional buoyant convection in a rectangular box with electrically conducting walls in the presence of a strong, horizontal magnetic field has been considered. The electric conductance of the six walls is arbitrary. An asymptotic solution to the problem in the inertialess and small Peclet number approximations has been obtained for high values of the Hartmann number, *Ha*. The solution is valid for an arbitrary temperature distribution resulting from both differential heating of walls and internal heat sources. The three-dimensional flow is characterised by the presence of high-velocity jets at the vertical walls of the cavity. The velocity of the jets is $O(Ha^{1/2})$ times higher than in the bulk of the fluid. For sufficiently high boxes, comparison of the velocity profiles in the middle of a box with fully developed solutions developed previously for infinitely long rectangular ducts gives excellent agreement. Properties of convective flows have been investigated and examples for various temperature distributions have been presented. It has been shown that for wall conductance ratios ~0.1, the three-dimensional effects are confined to about one value of the characteristic dimension of the duct cross-section at the top and the bottom of the box. The flow pattern has been shown to be very sensitive to symmetries of temperature and to variations of the wall conductance ratios. This property may be used to optimise the convective flow pattern. The numerical code developed on the basis of the asymptotic model is a flexible, fast tool to analyse and optimise convective flows in various blanket designs.

Dreidimensionale Konvektion in einer quaderförmigen Geometrie mit dünnen leitenden Wänden in einem starken horizontalen Magnetfeld

Zusammenfassung

In diesem Bericht werden dreidimensionale Konvektionsströmungen in quaderförmigen Geometrien mit elektrisch leitenden Wänden in einem horizontalen Magnetfeld untersucht. Die elektrische Leitfähigkeit der sechs Wände ist beliebig. Für große Hartmann Zahlen Ha wurden asymptotische Lösungen für trägheitsfreie Strömungen bei kleinen Peclet Zahlen ermittelt. Diese Lösungen gelten für beliebige Temperaturverteilungen, entstanden durch unterschiedlich beheizte Wände und/oder durch volumetrisch freigesetzte interne Beheizung. Die dreidimensionale Strömung ist charakterisiert durch Jets mit hohen Geschwindigkeiten entlang vertikaler Wände. Die Geschwindigkeit im Jet ist $O(Ha^{1/2})$ höher als im Kern der Strömung. Für sehr lange Kavitäten ergibt ein Vergleich der Strömung in der Mittelebene mit der einer voll entwickelten Strömung eine sehr gute Übereinstimmung. Es wurden Strömungsgrößen für verschiedene Temperaturverteilungen bestimmt. Es konnte gezeigt werden, dass für Wandleitparameter ~0.1 dreidimensionale Strömungsbereiche auf die unmittelbare Nähe der oberen und unteren Enden der Geometrie beschränkt sind. Die Strömungsverteilung reagiert sehr sensitiv auf Symmetrien des Temperaturfeldes und auf die Variation der Leitfähigkeit der Wände. Diese Eigenschaft könnte zur Optimierung der Konvektionsströmung genutzt werden. Das entwickelte numerische Rechenprogramm auf der Basis eines asymptotischen Modells ist ein flexibles und schnelles Werkzeug zur Berechnung konvektiver Strömungen für verschiedenste Blanket-Designs.

Three-dimensional buoyant convection in a rectangular box with thin conducting walls in a strong horizontal magnetic field

Contents

1 Introduction

Buoyant convection in cavities in the presence of an applied magnetic field received considerable attention due to its relevance to semiconductor crystal growth and liquid metal blankets for fusion reactors. For applications in nuclear fusion buoyant flows are dominant in blankets with separate cooling. In such blankets the liquid lithium-lead alloy Li17Pb83 serves mainly as breeding material while the heat is removed by another coolant. Such blankets do not need high velocities as those required in self-cooled blankets, where the fluid serves both as breeder and coolant simultaneously. For this reason pressure drop is not a serious issue for separately cooled blankets. A weak circulation of the fluid, however, is desired either by forced or buoyant convection in order to move the breeding product, tritium, out of the blanket. Stagnant fluid domains could accumulate tritium and cause safety problems. A properly designed blanket aims to avoid stagnant zones.

Two main candidates of separately cooled lithium- lead blankets have been considered in the past. The one which was developed to the most detail is the European *Water Cooled Lithium Lead* blanket (WCLL) (Giancarli et al (1992), Fütterer et al (2000)). In that blanket the breeder is confined in long vertical rectangular boxes, similar to the geometries investigated in this report. The heat is removed from the blanket by water flowing in cooling tubes which are inserted into the boxes. From a thermal point of view this blanket has internal heat sources due to volumetric heating and local heat sinks at the cooling tubes. This arrangement leads to non-uniform temperatures in horizontal cross sections that give rise to thermally induced buoyant convection.

The second candidate is the recently proposed *Helium Cooled Lithium Lead* blanket (HCLL). This blanket consists mainly of rectangular, liquid metal filled boxes, the walls of which are cooled internally by a high-pressure helium flow. With respect to geometry and thermal boundary conditions the latter design agrees perfectly with the geometries considered here since there are no internal obstacles inside the boxes as it was the case in WCLL. The internally released heat is transported mainly by thermal diffusion to the walls where it is removed by the helium.

During operation all liquid metal blankets are exposed to a strong horizontal magnetic field confining the fusion plasma. In the presence of a magnetic field the flow of an electrically conducting liquid metal induces electric currents, which themselves interact with the magnetic field. Usually this electromagnetic interaction results in strong braking of the liquid motion, especially in the core of the flow occupying almost the entire box. In some flow subregions, however, especially in the so-called parallel layers along the electrically conducting walls aligned with the magnetic field, electromagnetic interaction may drive the flow at high velocities. The buoyancy-induced velocities in the core and moreover the

velocities driven in the parallel layers are of same or higher order of magnitude as the forced flow required for safe tritium extraction. In order to improve knowledge about magneto-convective flows in fusion relevant geometries in strong magnetic fields such flows are analysed in the present report.

Buoyant convection has been studied by many authors, namely Hjellming & Walker (1987), Ozoe & Okada (1989), Okada & Ozoe (1992), Garandet, Alboussière & Moreau (1992), Alboussière, Garandet & Moreau (1993), (1996), Bojarevics (1995), Ma & Walker (1995), Tagawa & Ozoe (1997), (1998), Ben Hadid & Henry (1997), Ben Hadid, Henry & Kaddeche (1997), Bühler (1998), DiPiazza & Bühler (1999), Aleksandrova (2001) and Aleksandrova & Molokov (2000), (2002) among others. See reviews by Bühler (1998), Walker (1999) and Aleksandrova (2001) for more details. Below we give a brief overview of previous studies most relevant to the present investigation.

Perhaps the most important property of the buoyant flow in the presence of the magnetic field has been noted by Ma & Walker (1995) and Alboussière, Garandet & Moreau (1996). In both investigations solid walls were considered to be electrically insulating. They have shown that the magnitude of the induced flow may differ by orders of magnitude depending on whether the temperature is symmetric or anti-symmetric in the direction of the magnetic field.

The reason for this is in the closure pattern of the electric current. If the induced current is forced to flow through the Hartmann layers, they become active. They induce a potential difference in the core, which drives velocity of much higher magnitude than that induced originally by buoyancy. If currents bypass the Hartmann layers, no such high velocities are induced, and the convective flow remains highly damped by the field.

These ideas have been further developed by Aleksandrova (2001) and Aleksandrova & Molokov (2002), who gave complete classification of flows in closed cavities with electrically insulating walls for both vertical and horizontal magnetic fields. It has been shown that the flow pattern in the buoyant convective flow depends on many factors, such as the orientation of the field with respect to gravity, thermal conductance of the walls, symmetries of temperature in all three co-ordinates, the average values of the heat fluxes in all three directions, etc.

Flows in closed geometries with conducting walls have been studied mostly numerically (Tagawa & Ozoe (1998), DiPiazza & Bühler (1999)). Concerning analytical studies, Bühler (1998) investigated fully developed flow in long vertical rectangular ducts with thin conducting walls in a strong, horizontal magnetic field. The temperature distribution was arbitrary, independent of the vertical co-ordinate. It has been shown that symmetries of temperature are also important. Bühler (1998) presented various examples of flows owing to differential heating of duct walls, as well as volumetric heat sources. He has shown that jets in

the parallel layers at the walls parallel to the field are present, and that they may exist even if duct walls are perfect conductors.

As in hybrid liquid metal blankets ducts have a finite height, it is important to understand the resulting three-dimensional effects of the top and the bottom of the blanket. Therefore in this investigation we will be concerned with the steady, three-dimensional, convective flow in a rectangular box with thin, electrically conducting walls in the presence of a strong, horizontal magnetic field. The analysis is performed using an asymptotic flow model for high values of the Hartmann number.

2 Formulation

Consider the steady flow of a viscous, electrically conducting, incompressible fluid in a rectangular box (Fig. 1) in a strong, uniform magnetic field $\mathbf{B}^* = B_0^*\hat{\mathbf{y}}$. The box has a height of $2d^*$, and horizontal dimensions of $2a^*$ and $2l^*$ in the y- and x- directions, respectively (here x^*, y^*, z^* are Cartesian co-ordinates). Dimensional quantities are denoted by letters with asterisks, while their dimensionless counterparts - with the same letters, but without the asterisks. The walls of the box are numbered from 1 to 6 as shown in Fig. 1. Walls 1 and 2 are called the Hartmann walls, as they are transverse to the field, while those numbered 3-6 are called the parallel walls. All walls of the box are electrically conducting with electrical conductivity σ_i^* and thickness h_i^*, i = 1–6.

The box may be heated both externally and by internal volumetric heat sources Q^*. In the following we will be concerned with buoyant convective flow, which sets in owing to differences in temperature T^* implying variable density ρ^* within the fluid. Assuming that the Boussinesq approximation is valid, the fluid density is expressed in terms of temperature as follows:

$$\rho^* = \rho_0^*\left[1-\beta^*(T^*-T_0^*)\right].$$

The density of the fluid at temperature T_0^* is denoted by ρ_0^*, and the thermal expansion coefficient by β^*. Here T_0^* is a reference temperature at a certain, fixed point within the flow. The electrical conductivity, σ^*, and kinematic viscosity, ν^*, are assumed to be constant, independent of temperature.

Then the steady, dimensionless, inductionless equations governing the problem are (Bühler (1998)):

$$Ha^{-2}\nabla^2\mathbf{v} + \mathbf{j}\times\hat{\mathbf{y}} + T\hat{\mathbf{z}} = \nabla p + GrHa^{-4}(\mathbf{v}\cdot\nabla)\mathbf{v}, \tag{2.1}$$

$$\mathbf{j} = -\nabla\phi + \mathbf{v}\times\hat{\mathbf{y}}, \tag{2.2}$$

$$\nabla\cdot\mathbf{j} = 0, \tag{2.3}$$

$$\nabla \cdot \mathbf{v} = 0, \tag{2.4}$$

$$\nabla^2 T = Pe(\mathbf{v} \cdot \nabla)T - Q. \tag{2.5}$$

Here the length, the fluid velocity $\mathbf{v} = u\hat{\mathbf{x}} + v\hat{\mathbf{y}} + w\hat{\mathbf{z}}$, the electric current density $\mathbf{j}$, and the electric potential ϕ are normalised by a^*, $v_0^* = \rho_0^* \beta^* g^* \Delta T^* / (\sigma^* B_0^{*2})$, $\sigma^* v_0^* B_0^*$, and $a^* v_0^* B_0^*$, respectively; g^* is the intensity of gravity. The characteristic temperature difference ΔT^* depends on the nature of the heating. It may be specified either in terms of external heat flux, applied temperature difference at the walls, or characteristic intensity of internal heat sources. The dimensionless temperature, T, and pressure, p, are defined as follows: $T = (T^* - T_0^*)/(\Delta T^*)$, $p = (p^* + z^* \rho_0^* g^*)/(v_0^* \sigma^* B_0^{*2} a^*)$.

The ratio of the electromagnetic to the viscous forces is determined by the square of the Hartmann number,

$$Ha = B_0^* a^* \sqrt{\sigma^* / \rho_0^* \nu^*},$$

which is supposed to be sufficiently high here for viscous effects to be confined to thin boundary layers.

The Grashof number,

$$Gr = a^{*3} \beta^* g^* \Delta T^* / \nu^{*2}$$

characterises the importance of the buoyancy forces. Parameter Gr/Ha^2 plays the role of the Reynolds number, Re, while Ha^4/Gr plays that of the interaction parameter, N (Alboussière, Garandet & Moreau (1996), Bühler (1998)). It is assumed here that the flow is inertialess in all the flow subregions. This requires $Gr << Ha^{5/2}$, which is equivalent to $N >> Ha^{3/2}$, as in duct flows with thin conducting walls. In a helium-cooled PbLi blanket typical values of dimensional parameters are: $a^* = 0.1\text{m}$, $\Delta T^* = 100K$, $B_0^* = 10T$. Thus for Li17Pb83 at $T_0^* = 673K$ one gets $Ha \sim 2.5 \cdot 10^4$ and $Gr \sim 10^9$ - $2 \cdot 10^{10}$, so that the inertialess condition is fulfilled. For lower magnetic fields, e.g. for the outboard blanket, inertial effects might play a certain role. In any case, since blanket walls are electrically conducting, inertial effects, if present, are expected to be confined to parallel layers in the 3-D regions at the top and the bottom of the box. Thus the influence of inertia on the global flow in the core will be small even if $Gr \sim Ha^{5/2}$.

The Peclet number,

$$Pe = v_0^* a^* / \kappa^* = \rho_0^* \beta^* g^* \Delta T^* a^* / (\kappa^* \sigma^* B_0^{*2})$$

determines the ratio of convective and conductive heat fluxes. In the above κ^* is the thermal conductivity of the fluid. The Peclet number can be expressed as follows:

$$Pe = \text{Pr}\, GrHa^{-2},$$

where $Pr = \nu^* / \kappa^*$ is the Prandtl number. For a sufficiently strong magnetic field Pe becomes sufficiently small to neglect convective heat transfer in Eq. (2.5). Thus the temperature distribution becomes independent of the fluid flow, while the energy equation reduces to

$$\nabla^2 T = -Q\,. \tag{2.6}$$

Eq. (2.6) is solved subject to the thermal boundary conditions. For each wall this may be either a specified heat flux or a fixed temperature. Specific conditions will be introduced when examples of various flows will be considered. Once T is known, it enters as the source term in Eq. (2.1). Thus, for the hydrodynamic part of the problem the temperature distribution is supposed to be given.

With these assumptions Eqs. (2.1)-(2.4) become:

$$Ha^{-2}\nabla^2 u - j_z = \frac{\partial p}{\partial x}, \quad Ha^{-2}\nabla^2 v = \frac{\partial p}{\partial y}, \quad Ha^{-2}\nabla^2 w + j_x = \frac{\partial p}{\partial z} - T\,, \tag{2.7a-c}$$

$$j_x = -\frac{\partial \phi}{\partial x} - w\,, \quad j_y = -\frac{\partial \phi}{\partial y}, \quad j_z = -\frac{\partial \phi}{\partial z} + u\,, \tag{2.8a-c}$$

$$\frac{\partial u}{\partial x} + \frac{\partial v}{\partial y} + \frac{\partial w}{\partial z} = 0\,, \quad \frac{\partial j_x}{\partial x} + \frac{\partial j_y}{\partial y} + \frac{\partial j_z}{\partial z} = 0\,. \tag{2.9a,b}$$

The boundary condition for the fluid velocity at each wall is the no-slip condition

$$\mathbf{v} = 0. \tag{2.10}$$

The walls are supposed to be thin and electrically conducting. Thus,

$$\mathbf{j}\cdot\hat{\mathbf{n}}_i = c_i \nabla_i^2 \phi_i \quad \text{at all walls, } i = 1\text{-}6, \tag{2.11}$$

where $\hat{\mathbf{n}}_i$ is the normal unit vector to the wall i into the fluid, $c_i = \sigma_i^* h_i^* / \sigma^* a^*$ is the wall conductance ratio, and ∇_i^2 is the Laplace operator in the plane on wall i.

It will be assumed further that $c_{1,2} >> Ha^{-1}$, $c_{3\text{-}6} >> Ha^{-1/2}$, i.e. all the walls are much better conductors than the adjacent layers (Sec. 3). For a helium-cooled PbLi blanket this condition is fulfilled, as typically $c \sim 0.07$.

The volume flux through any (x,y)-cross-section S of the box must vanish, which gives:

$$\iint_S w\,dy\,dx = 0 \quad \text{for any } z = \text{constant}. \tag{2.12}$$

Substituting Eq. (2.8a) into Eq. (2.7c), integrating the result over S, and using Eq. (2.12) yields:

$$Ha^{-2}\oint_\Lambda \frac{\partial w}{\partial n} d\Lambda + Ha^{-2}\iint_S \frac{\partial^2 w}{\partial z^2}\,dx\,dy + \int_{-1}^{1}[\phi_4 - \phi_3]\,dy = \iint_S \frac{\partial p}{\partial z}\,dx\,dy - \overline{T}(z)\,, \tag{2.13}$$

where Λ is the boundary of S, and

$$\overline{T}(z) = \iint_S T\,dx\,dy$$

is the dimensionless net buoyancy force in the cross-section S. It will be shown in Sec. 3 that the first two terms in the above equation are at most $O(Ha^{-1})$, i.e. much smaller than the other ones. Neglecting these terms gives:

$$\iint_S \frac{\partial p}{\partial z}\,dxdy = \overline{T}(z) - \int_{-1}^{1}[\phi_3 - \phi_4]dy \quad \text{for any } z = \text{constant.} \tag{2.14}$$

Eq. (2.14) may be interpreted as follows: at any cross-section of the box z = constant such a net vertical pressure gradient is induced to compensate the net buoyancy force and the difference between potentials of walls 3 and 4 that the total volume flux is zero.

In Sec. 3 Eqs. (2.7) - (2.9) subject to the conditions (2.10), (2.11), (2.14) are solved for a given temperature by the method of matched asymptotic expansions at high values of the Hartmann number. Generally, only leading terms in the asymptotic expansions in each flow subregion are presented.

3 Asymptotic solution for *Ha* >> 1

For $Ha >> 1$ the interior of the cavity can be divided into several subregions (Fig. 1), where the flow is governed by the reduced equations. The most important of the subregions, which determine the flow pattern, are the inviscid core *C*, occupying the bulk of the flow, the Hartmann layers *H1, H2* of thickness $O(Ha^{-1})$ at the walls 1 and 2 perpendicular to the magnetic field, parallel layers *Pi* of thickness $O(Ha^{-1/2})$ at the walls i = 3-6 parallel to the magnetic field, and the corner parallel layers with dimensions $O(Ha^{-1/2})\times O(1)\times O(Ha^{-1/2})$. The latter are formed at the intersection of layers *Pi*. As has been discussed by Molokov & Bühler (1994), the details of the flow in the corner parallel layers are not important, and thus they will not be considered further.

3.1 Core *C*

In the core viscous terms in Eqs. (2.7) may be neglected. Then from Eq. (2.7b) follows that the core pressure is a function of x and z only. This fact is used to integrate reduced Eqs. (2.7)-(2.9) with respect to y. As a result of integration, the core variables may be represented in the form used by Aleksandrova (2001) as follows:

$$p_C = P(x,z)\,, \tag{3.1}$$

$$\phi_C = \Phi(x,z) - y\cdot J_y(x,z) - M_x(x,y,z)\,, \tag{3.2}$$

$$j_{x,C} = \frac{\partial P}{\partial z} - T(x,y,z), \quad j_{y,C} = J_y(x,z) + \int_0^y \frac{\partial T}{\partial x}(x,t,z)dt, \quad j_{z,C} = -\frac{\partial P}{\partial x}, \quad (3.3a\text{-}c)$$

$$u_C = -\frac{\partial P}{\partial x} + \frac{\partial \phi_C}{\partial z}, \tag{3.4}$$

$$v_C = V_y(x,z) + y\nabla_{xz}^2 P - \int_0^y \frac{\partial T}{\partial z}(x,t,z)dt, \tag{3.5}$$

$$w_C = T(x,y,z) - \frac{\partial P}{\partial z} - \frac{\partial \phi_C}{\partial x}, \tag{3.6}$$

where

$$M_x(x,y,z) = \int_0^y (y-t)\frac{\partial T}{\partial x}(x,t,z)dt. \tag{3.7}$$

Throughout this paper subscripts *C, Pi* and *Hi* of the flow variables denote the flow subregion, i.e. the core, the parallel- and the Hartmann-layers, where corresponding limit equations are valid. Variables with these subscripts are $O(1)$.

In Eqs. (3.1)-(3.6) there are four unknown functions of x and z. These are the core pressure P, the electric potential Φ at $y = 0$, and the y-components of current J_y and velocity V_y at $y = 0$. In the following all the core variables will be expressed in terms of wall potentials ϕ_i and core pressure P. As there is no jump in the $O(1)$ electric potential across the Hartmann layers, then the core potential evaluated at $y = \pm 1$ equals that of walls 1 and 2, respectively. This fact and Eq. (3.2) yield:

$$J_y = \tfrac{1}{2}\left\{\phi_2 - \phi_1 + \int_{-1}^{1}[y - sign(y)]\frac{\partial T}{\partial x}dy\right\}$$

$$= \tfrac{1}{2}\{\phi_2 - \phi_1\} - \tilde{M}_x(x,1,z), \tag{3.8}$$

$$\Phi = \tfrac{1}{2}\left\{\phi_2 + \phi_1 + \int_{-1}^{1}(1-|y|)\frac{\partial T}{\partial x}dy\right\}$$

$$= \tfrac{1}{2}\{\phi_2 + \phi_1\} + \hat{M}_x(x,1,z). \tag{3.9}$$

Symbols ˜ and ˆ above M_x mean that either an odd, $\tilde{T}$, or an even, $\hat{T}$, part of temperature with respect to y, respectively, is used in Eq. (3.7).

Then the y-component of core current and the core potential become:

$$j_{y,C} = \tfrac{1}{2}\{\phi_2 - \phi_1\} - \tilde{M}_x(x,1,z) + \int_0^y \frac{\partial T}{\partial x}(x,t,z)dt, \tag{3.10}$$

$$\phi_C = \phi_L + \hat{M}_x(x,1,z) + y\tilde{M}_x(x,1,z) - M_x(x,y,z)\,, \tag{3.11}$$

where

$$\phi_L = \tfrac{1}{2}(\phi_1 + \phi_2) + y\,\tfrac{1}{2}(\phi_1 - \phi_2)\,. \tag{3.12}$$

The normalization condition (2.14) gives:

$$2\int_{-l}^{l}\frac{\partial P}{\partial z}dx = \overline{T}(z) - \int_{-1}^{1}[\phi_3 - \phi_4]dy \quad \text{for any } z = \text{constant}. \tag{3.13}$$

As there are four unknown functions in the core, namely P, V_y, ϕ_1 and ϕ_2, four equations are required to determine them. They are provided by the conditions of matching with the Hartmann-layer solutions. In Sec. 3.2 these equations will be derived for arbitrary values of $c_{1,2}$, including $c_{1,2} = 0$ (insulating walls). Further, however, it will be assumed that $c_{1,2} >> Ha^{-1}$.

3.2 Hartmann layers *H1* and *H2*

As there are no jets in the Hartmann layers, the $O(1)$ core velocity must satisfy the non-penetration conditions at $y = \pm 1$. This gives the first two equations on the core variables, namely:

$$v_C = 0 \quad \text{at } y = \pm 1. \tag{3.14}$$

Then from Eqs. (3.5) and (3.14) follows:

$$V_y = \frac{1}{2}\int_{-1}^{1}\frac{\partial T}{\partial z}sign(y)dy\,, \tag{3.15}$$

$$\nabla_{xz}^2 P = \frac{1}{2}\int_{-1}^{1}\frac{\partial T}{\partial z}dy\,. \tag{3.16}$$

Eq. (3.16) is the governing equation for the core pressure.

Substituting expressions (3.15) and (3.16) into Eq. (3.5) gives:

$$v_C = \frac{1}{2}(y+1)\int_{0}^{1}\frac{\partial T}{\partial z}dy + \frac{1}{2}(y-1)\int_{-1}^{0}\frac{\partial T}{\partial z}dy - \int_{0}^{y}\frac{\partial T}{\partial z}(x,t,z)dt\,. \tag{3.17}$$

Thus the y-component of the core velocity is readily available. It is a function of temperature only.

To derive the other two boundary conditions for the core variables at $y = \pm 1$ only Eqs. (2.7a,c), (2.8a,c) and (2.9b) will be used. We will consider first layer *H1* at $y = 1$ and introduce a stretched variable $y_{H1} = Ha(y - 1)$. Then Eqs. (2.7a,c), (2.8a,c) yield:

$$\frac{\partial^2 u_{H1}}{\partial y_{H1}^2} - u_{H1} = -\frac{\partial \phi_1}{\partial z} + \frac{\partial P}{\partial x}, \tag{3.18}$$

$$\frac{\partial^2 w_{H1}}{\partial y_{H1}^2} - w_{H1} = \frac{\partial \phi_1}{\partial x} + \frac{\partial P}{\partial z} - T\big|_{y=1}. \tag{3.19}$$

The solution to these equations, which satisfies the no-slip condition at the wall $y = 1$, is:

$$u_{H1} = \left(\frac{\partial \phi_1}{\partial z} - \frac{\partial P}{\partial x} \right)(1 - e^{y_{H1}}), \tag{3.20}$$

$$w_{H1} = \left(-\frac{\partial \phi_1}{\partial x} - \frac{\partial P}{\partial z} + T\big|_{y=1} \right)(1 - e^{y_{H1}}). \tag{3.21}$$

From the current conservation law (2.9b) and Eqs. (2.8a,c), (3.18) and (3.19) follows that

$$Ha \frac{\partial j_{y,H1}}{\partial y_{H1}} = \nabla_{xz}^2 \phi_1 e^{y_{H1}} + \left. \frac{\partial T}{\partial x} \right|_{y=1} (1 - e^{y_{H1}}). \tag{3.22}$$

Integrating Eq. (3.22) with respect to y_{HI}, using the boundary condition (2.11) for $i = 1$, and matching the y-component of the core current given by Eq. (3.10) to that in the Hartmann layer, results in the equation for wall potential ϕ_1 as follows:

$$\bar{c}_1 \nabla_{xz}^2 \phi_1 + \tfrac{1}{2}(\phi_2 - \phi_1) = -\frac{1}{2} \int_{-1}^{1} \frac{\partial T}{\partial x}(1 + y) dy + Ha^{-1} \left. \frac{\partial T}{\partial x} \right|_{y=1}, \tag{3.23}$$

where $\bar{c}_1 = c_1 + Ha^{-1}$ is the efficient conductance ratio of wall 1.

The Hartmann layer at wall 2 is treated in a similar way and yields a similar equation for ϕ_2 as follows:

$$\bar{c}_2 \nabla_{xz}^2 \phi_2 + \tfrac{1}{2}(\phi_1 - \phi_2) = -\frac{1}{2} \int_{-1}^{1} \frac{\partial T}{\partial x}(1 - y) dy + Ha^{-1} \left. \frac{\partial T}{\partial x} \right|_{y=-1}, \tag{3.24}$$

where $\bar{c}_2 = c_2 + Ha^{-1}$ is the efficient conductance ratio of wall 2.

Eqs. (3.23) and (3.24) are valid for both conducting and insulating Hartmann walls. As has been discussed by Aleksandrova (2001), the terms $Ha^{-1}\partial T/\partial x (y = \pm 1)$ in the right hand side of Eqs. (3.23) and (3.24) represent the y-component of the *curl* of the buoyancy force at the boundary between the core region and the Hartmann layers. They are important for insulating walls (or more generally, for $c_{1,2} = O(Ha^{-1})$) only. It is necessary to retain these terms in that case in order to ensure conservation of current $O(Ha^{-1})$ in the Hartmann layers.

In the following we will be concerned with walls 1 and 2 being much better conductors than the Hartmann layers ($c_{1,2} >> Ha^{-1}$). Thus in Eqs. (3.23), (3.24) parameter $\bar{c}_{1,2}$ will be replaced by $c_{1,2}$, while terms $Ha^{-1}\partial T/\partial x (y = \pm 1)$ will be neglected.

3.3 Electric potentials of parallel walls 3-6

Owing to the assumption $c_{3-6} >> Ha^{-1/2}$, there is no jump of the normal component of the electric current across the parallel layers (Hua et al. (1988)). Thus, expressions for the *x*- and *z*- components of core current given by Eqs. (3.3a,c) may be substituted directly into Eq. (2.11) with *i* = 3,4 and 5,6, respectively. This gives equations governing potentials of walls 3-6 as follows:

$$c_{3,4}\nabla^2_{yz}\phi_{3,4} = \mp\frac{\partial P}{\partial z}\bigg|_{x=\pm l} \pm T(\pm l, y, z), \tag{3.25}$$

$$c_{5,6}\nabla^2_{xy}\phi_{5,6} = \pm\frac{\partial P}{\partial x}\bigg|_{z=\pm d}. \tag{3.26}$$

Thus equations for the wall potentials $\phi_{3\text{-}6}$ have been obtained with no reference to the parallel layers at all.

At the junction between walls electric potential must be continuous. Since all walls are supposed to be better conductors than the adjacent Hartmann- or parallel- layers, the electric current leaving one wall must enter the adjacent wall. Thus if walls *i* and *j* have a common boundary Γ_{ij}, then

$$\phi_i = \phi_j, \quad c_i\frac{\partial\phi_i}{\partial\eta_i} = -c_j\frac{\partial\phi_j}{\partial\eta_j} \quad \text{along } \Gamma_{ij}, \tag{3.27}$$

where η_i, η_j are normal, inward derivatives to Γ_{ij} in the planes of walls *i* and *j*, respectively.

Finally, to determine the boundary conditions for the core pressure, which obeys Eq. (3.16), parallel layers need to be considered.

3.4 Parallel layers *P3, P4*

Flow in parallel layers is characterized by the presence of $O(Ha^{1/2})$ high velocity jets tangential to parallel walls. Consider first parallel layer *P3* at $x = l$. The stretched co-ordinate is $\xi = Ha^{1/2}(x-l)$, while the scaling of the flow variables is as follows: *w, v* are $O(Ha^{1/2})$, *u*, j_z, j_y and ϕ are $O(1)$, $j_x = j_{x,C}(x=l) + Ha^{-1/2}j_{x,P3}$, $p = P(x=l) + Ha^{-1/2}p_{P3}$. Although it is possible to solve the parallel-layer equations exactly, we will restrict ourselves to the derivation of the boundary conditions for the core pressure, and the analysis of the integral characteristics of the parallel layers, such as local flow rates (Molokov&Bühler (1994)).

Introducing scaled variables into Eq. (2.8a) and retaining leading terms as $Ha \to \infty$ gives:

$$w_{P3} = -\frac{\partial \phi_{P3}}{\partial \xi}. \tag{3.28}$$

Integrating this equation over the layer with respect to ξ yields the z-component of the local flow rate carried by layer *P3* as follows:

$$q_{z,3}(y,z) = \int_{-\infty}^{0} w_{P3} d\xi = \phi_C(x=l) - \phi_3, \tag{3.29}$$

i.e. for given y and z the amount of fluid carried by the jet in layer *P3* in the z-direction is proportional to the jump in the electric potential across the layer, a well-known fact.

Now, Eqs. (2.7a), (2.8c) and (2.9a) give:

$$j_{z,P3} = -\frac{\partial p_{P3}}{\partial \xi}, \quad u_{P3} = \frac{\partial \phi_{P3}}{\partial z} + j_{z,P3}, \quad \frac{\partial u_{P3}}{\partial \xi} + \frac{\partial v_{P3}}{\partial y} + \frac{\partial w_{P3}}{\partial z} = 0. \tag{3.30a-c}$$

Eliminating w_{P3}, u_{P3}, ϕ_{P3} and $j_{z,P3}$ from Eqs. (3.28) and (3.30) results in the following equation:

$$\frac{\partial^2 p_{P3}}{\partial \xi^2} = \frac{\partial v_{P3}}{\partial y}. \tag{3.31}$$

Integrating this equation with respect to ξ over the layer, and using matching conditions with the core and Eqs. (3.30a,b) gives:

$$\frac{\partial \phi_3}{\partial z} - \left.\frac{\partial P}{\partial x}\right|_{x=l} = \int_{-\infty}^{0} \frac{\partial v_{P3}}{\partial y} d\xi. \tag{3.32}$$

Integrating further Eq. (3.32) with respect to y between –1 and 1, gives the following boundary condition for the core pressure:

$$\frac{\partial P}{\partial x} = \frac{1}{2}\int_{-1}^{1} \frac{\partial \phi_3}{\partial z} dy \quad \text{at } x = l. \tag{3.33}$$

If integration of Eq. (3.31) is performed between –1 and y, and use of Eq. (3.32) is made, the result is the local flow rate $q_{y,3}$ in the y-direction, namely:

$$q_{y,3} = \int_{-\infty}^{0} v_{P3} d\zeta_3 = \int_{-1}^{y} \frac{\partial \phi_3}{\partial z} dy - \frac{1}{2}(y+1)\int_{-1}^{1} \frac{\partial \phi_3}{\partial z} dy. \tag{3.34}$$

For $c_3 < \infty$ the expression $-\partial \phi_3 / \partial z$ is proportional to the wall current flowing in the z-direction. Thus expression (3.34) may be interpreted as follows. Local flow rate $q_{y,3}$ is proportional to the deviation of current flowing in the z-direction from being independent of y. If ϕ_3 is at most a linear function of z, then $q_{y,3}$ vanishes in the whole layer. This happens, for example, if wall 3 is a perfect conductor.

The analysis of parallel layer *P4* gives similar expressions for the boundary condition for the core pressure and the local flow rate, namely:

$$\frac{\partial P}{\partial x} = -\frac{1}{2}\int_{-1}^{1}\frac{\partial \phi_4}{\partial z}dy \quad \text{at } x = -l, \tag{3.35}$$

$$q_{z,4}(y,z) = \phi_4 - \phi_C(x=-l), \tag{3.36}$$

$$q_{y,4}(y,z) = -\int_{-1}^{y}\frac{\partial \phi_4}{\partial z}dy + \frac{1}{2}(y+1)\int_{-1}^{1}\frac{\partial \phi_4}{\partial z}dy. \tag{3.37}$$

3.5 Parallel layers *P5, P6*

Consider now layer *P5* at $z = d$. The stretched co-ordinate is: $\zeta = Ha^{1/2}(z-d)$, while the scaling of the flow variables is as follows: *u, v* are $O(Ha^{1/2})$, *w*, j_x, j_y and ϕ are $O(1)$, $j_z = j_{z,C}(z=d) + Ha^{-1/2} j_{z,P5}$, $p = P(z=d) + Ha^{-1/2} p_{P5}$.

Introducing scaled variables into Eqs. (2.8c), (2.7a,c), (2.9a) and retaining leading terms as $Ha \to \infty$ gives:

$$u_{P5} = \frac{\partial \phi_{P5}}{\partial \zeta}, \quad j_{x,P5} = \frac{\partial p_{P5}}{\partial \zeta} - T(x,y,d), \tag{3.38a,b}$$

$$w_{P5} = -\frac{\partial \phi_{P5}}{\partial x} - j_{x,P5}, \quad \frac{\partial u_{P5}}{\partial x} + \frac{\partial v_{P5}}{\partial y} + \frac{\partial w_{P5}}{\partial \zeta} = 0. \tag{3.39a,b}$$

From Eqs. (3.38) and (3.39) follows:

$$q_{x,5}(x,y) = \phi_5 - \phi_C(z=d), \tag{3.40}$$

and

$$\frac{\partial^2 p_{P5}}{\partial \zeta^2} = \frac{\partial v_{P5}}{\partial y}. \tag{3.41}$$

Integrating this equation with respect to ζ over the layer, and using matching conditions with the core and Eqs. (3.38b), (3.39a), gives:

$$T(x,y,d) - \frac{\partial \phi_5}{\partial x} - \left.\frac{\partial P}{\partial z}\right|_{z=d} = \int_{-\infty}^{0}\frac{\partial v_{P5}}{\partial y}d\zeta. \tag{3.42}$$

Integrating Eq. (3.42) with respect to *y* between –1 and 1, gives the following boundary condition for pressure:

$$\frac{\partial P}{\partial z} = -\frac{1}{2}\int_{-1}^{1}\frac{\partial \phi_5}{\partial x}dy + \frac{1}{2}\int_{-1}^{1}T dy \quad \text{at } z = d. \tag{3.43}$$

If integration of Eq. (3.42) is performed between –1 and *y*, and use of Eq. (3.43) is made, the result is the local flow rate $q_{y,5}$ in the *y*-direction, namely:

$$q_{y,5} = \int_{-\infty}^{0} v_{P5} d\zeta = \int_{-1}^{y} \left[T(x,t,d) - \frac{\partial \phi_5}{\partial x} \right] dt - \frac{1}{2}(y+1) \int_{-1}^{1} \left[\frac{\partial \phi_5}{\partial x} - T(x,y,d) \right] dy \,. \quad (3.44)$$

The analysis of parallel layer *P6* gives similar expressions for the boundary condition for the core pressure and the *y*-component of the local flow rate, $q_{y,6}$, namely:

$$\frac{\partial P}{\partial z} = \frac{1}{2} \int_{-1}^{1} \frac{\partial \phi_6}{\partial x} dy + \frac{1}{2} \int_{-1}^{1} T dy \quad \text{at } z = -d. \quad (3.45)$$

$$q_{y,6} = -\int_{-1}^{y} \left[T(x,t,-d) - \frac{\partial \phi_6}{\partial x} \right] dt + \frac{1}{2}(y+1) \int_{-1}^{1} \left[\frac{\partial \phi_6}{\partial x} - T(x,y,-d) \right] dy \,, \quad (3.46)$$

3.6 Summary

The problem for wall potentials and core pressure is now fully defined. It consists of Eqs. (3.16), (3.23)-(3.26) and boundary conditions (3.27), (3.33), (3.35), (3.43) and (3.45). The normalization condition is given by Eq. (3.13). For convenience we present the summary of the results in Table 1.

Table 1. Summary of the asymptotic results

Wall potentials and core pressure	
Equations	$$\nabla^2_{xz} P = \frac{1}{2}\int_{-1}^{1} \frac{\partial T}{\partial z}\, dy \qquad (3.47)$$
	$$c_{1,2}\nabla^2_{xz}\phi_{1,2} - \tfrac{1}{2}\phi_{1,2} = -\tfrac{1}{2}\phi_{2,1} - \frac{1}{2}\int_{-1}^{1} \frac{\partial T}{\partial x}(1 \pm y)\, dy \qquad (3.48)$$
	$$c_{3,4}\nabla^2_{yz}\phi_{3,4} = \mp \left.\frac{\partial P}{\partial z}\right|_{x=\pm l} \pm T(\pm l, y, z) \qquad (3.49)$$
	$$c_{5,6}\nabla^2_{xy}\phi_{5,6} = \pm \left.\frac{\partial P}{\partial x}\right|_{z=\pm d} \qquad (3.50)$$
Boundary conditions	$$\phi_i = \phi_j\,, \quad c_i \frac{\partial \phi_i}{\partial \eta_i} = -c_j \frac{\partial \phi_j}{\partial \eta_j} \quad \text{along } \Gamma_{ij} \qquad (3.51a,b)$$
	$$\frac{\partial P}{\partial x} = \pm \frac{1}{2}\int_{-1}^{1} \frac{\partial \phi_{3,4}}{\partial z}\, dy \quad \text{at } x = \pm l \qquad (3.52)$$
	$$\frac{\partial P}{\partial z} = \mp \frac{1}{2}\int_{-1}^{1} \frac{\partial \phi_{5,6}}{\partial x}\, dy + \frac{1}{2}\int_{-1}^{1} T\, dy \quad \text{at } z = \pm d \qquad (3.53)$$
Core variables	$$\phi_C = \phi_L + \hat{M}_x(x,1,z) + y\widetilde{M}_x(x,1,z) - M_x(x,y,z) \qquad (3.54)$$
	$$j_{x,C} = \frac{\partial P}{\partial z} - T \qquad (3.55)$$
	$$j_{y,C} = \tfrac{1}{2}\{\phi_2 - \phi_1\} - \widetilde{M}_x(x,1,z) + \int_0^y \frac{\partial T}{\partial x}(x,t,z)\, dt \qquad (3.56)$$
	$$j_{z,C} = -\frac{\partial P}{\partial x} \qquad (3.57)$$
	$$u_C = -\frac{\partial P}{\partial x} + \frac{\partial \phi_C}{\partial z} \qquad (3.58)$$
	$$v_C = \tfrac{1}{2}(y+1)\int_0^1 \frac{\partial T}{\partial z}\, dy + \tfrac{1}{2}(y-1)\int_{-1}^{0} \frac{\partial T}{\partial z}\, dy - \int_0^y \frac{\partial T}{\partial z}(x,t,z)\, dt \qquad (3.59)$$
	$$w_C = T - \frac{\partial P}{\partial z} - \frac{\partial \phi_C}{\partial x} \qquad (3.60)$$
Layers *P3, P4*, local flow rates	$$q_{z,3,4}(y,z) = \pm\left[\phi_C(x = \pm l) - \phi_{3,4}\right] \qquad (3.61)$$
	$$q_{y,3,4}(y,z) = \pm \int_{-1}^{y} \frac{\partial \phi_{3,4}}{\partial z}\, dy \mp \frac{1}{2}(y+1)\int_{-1}^{1} \frac{\partial \phi_{3,4}}{\partial z}\, dy \qquad (3.62)$$
Layers *P5, P6*, local flow rates	$$q_{x,5,6}(x,y) = \pm\left[\phi_{5,6} - \phi_C(z = \pm d)\right] \qquad (3.63)$$
	$$q_{y,5,6} = \pm \int_{-1}^{y}\left[T(x,t,\pm d) - \frac{\partial \phi_{5,6}}{\partial x}\right] dt \mp \frac{1}{2}(y+1)\int_{-1}^{1}\left[\frac{\partial \phi_{5,6}}{\partial x} - T(x,y,\pm d)\right] dy \qquad (3.64)$$

4 Numerical method

For a general temperature distribution and walls of finite conductance the system of equations governing wall potentials and core pressure is solved numerically. An iterative method is used as described by Molokov & Bühler (1994) and in more detail by Molokov & Bühler (1993).

Briefly, at each iteration step n Eqs. (3.47)-(3.50) are solved separately using a second-order accurate finite-difference scheme combined with a Fast Poisson Solver. The scheme has been used with 64 points per unit length in all calculations presented below. The values in the right hand sides of Eqs. (3.48)-(3.50), (3.52), (3.53) are taken from a previous iteration step.

For a wall potential ϕ_i (i = 1,…,6) at each iteration step the boundary conditions along Γ_{ij} are given by either Eq. (3.51a) or (3.51b). If for a wall i,

$$\phi_i^{(n)} = \phi_j^{(n-1)} \quad \text{along } \Gamma_{ij},$$

then for the wall j

$$\frac{\partial \phi_j^{(n)}}{\partial \eta_j} = -\frac{c_i}{c_j} \frac{\partial \phi_i^{(n-1)}}{\partial \eta_i}.$$

Under-relaxation is used in the Neumann boundary condition of the type above, especially for $c_j << 1$. The value of the under-relaxation parameter $\omega = 0.05$ was sufficient to achieve convergence in all cases presented here.

Iterations stopped when the maximal difference in the derivatives of the wall potentials at two successive iteration steps becomes below 10^{-10}.

5 Results and discussion

For insulating walls one or the other symmetry of temperature may lead to changes of the fluid velocity by $O(Ha^{1/2})$ or even by $O(Ha)$ in either the core or the parallel layers (Aleksandrova (2001)). If walls are electrically conducting, the velocity in the core is always $O(1)$, while that in parallel layers is at most $O(Ha^{1/2})$, so no such drastic changes of the flow pattern are expected. However, as follows from Table 1 symmetries of temperature with respect to all three co-ordinates still affect qualitatively the flow pattern in the core. The effect of these will be discussed in the next sections.

We split the discussion into two major sections depending on symmetry of the flow with respect to y. Within each section other symmetries with respect to x and z are discussed.

Further, in each section the discussion starts for boxes with certain walls being perfect conductors with the following aims. On the one hand, this helps (i) to understand the reason why certain walls are being active or passive in a sense that the values of their wall conductance ratios do or do not affect the flow; (ii) to understand the driving mechanism of the flow in various flow regions. On the other hand, in some experiments on buoyant convection heated and cooled walls are made of thick copper. Thus in the first approximation they may be considered as being perfectly conducting.

For various symmetries flow pattern is demonstrated on several examples of temperature distribution, which includes practically important cases of differentially heated walls and internal heat sources. These examples have been selected in such a way as to show the qualitative difference in the resulting flow pattern depending on either symmetries or thermal boundary conditions. Some of the examples of temperature variation may look artificial. However, as the problem is linear, temperature may be represented as a linear combination of functions, which are qualitatively similar to those used in the examples.

Calculations for the helium-cooled PbLi blanket will be performed once the design is fixed.

5.1 *y*-anti-symmetric case

If temperature is anti-symmetric in y and $c_1 = c_2$, all the core flow variables become either symmetric, or anti-symmetric in y. In particular, core pressure vanishes, while ϕ_C, $j_{x,C}$, w_C, u_C are anti-symmetric, while $j_{y,C}$ and v_C are symmetric. The volume flux condition (3.13) is satisfied automatically. In addition, from Eqs. (3.55) and (3.57) follows that

$$j_{x,C} = -\widetilde{T}\,, \quad j_{z,C} = 0\,, \tag{5.1a,b}$$

i.e. the core current flows in the (x,y)-planes, while the x-component of current is fully determined by temperature. All other flow variables depend not only on temperature directly, but on the wall potentials as well. The terms involving temperature in Eqs. (3.56) and (5.1b) represent the primary driving "force" for the core currents. Those terms involving wall potentials are secondary ones resulting from the necessity of the currents to complete their circuits in the conducting walls. In order to understand the flow better, we will consider first the case when the wall potentials vanish, i.e. all walls being perfect conductors.

5.1.1 All walls perfectly conducting

If all the walls are perfectly conducting ($c_i \to \infty$, i = 1,…,6), the solution for the core becomes expressed in terms of temperature only, and thus is known. It is given by Eqs. (5.1), (3.59) and the following expressions:

$$\phi_C = y\widetilde{M}_x(x,1,z) - \widetilde{M}_x(x,y,z)\,, \tag{5.2}$$

$$j_{y,C} = -\widetilde{M}_x(x,1,z) + \int_0^y \frac{\partial \widetilde{T}}{\partial x}(x,t,z)dt\,, \tag{5.3}$$

$$u_C = \frac{\partial \phi_C}{\partial z}\,, \quad w_C = \widetilde{T} - \frac{\partial \phi_C}{\partial x}\,, \tag{5.4a,b}$$

which follow from Eqs. (3.54), (3.56), (3.58) and (3.60).

From Eqs. (5.1) and (5.3) follows that the streamfunction for the core current is

$$\Psi_C = \int_0^y \widetilde{T}(x,t,z)dt - \int_0^1 (1-t)\widetilde{T}(x,t,z)dt\,, \tag{5.5}$$

where

$$j_{y,C} = \partial \Psi_C / \partial x\,, \quad j_{x,C} = -\partial \Psi_C / \partial y\,. \tag{5.6}$$

The expressions for the local flow rates in layers *P3-P6* are:

$$q_{z,3,4}(y,z) = \pm \phi_C(x = \pm l)\,, \quad q_{y,3,4}(y,z) = 0\,, \tag{5.7a,b}$$

$$q_{x,5,6}(x,y) = \mp \phi_C(z = \pm d)\,, \quad q_{y,5,6}(x,y) = \pm \int_{-1}^y \widetilde{T}(x,t,d)dt\,. \tag{5.8a,b}$$

From Eq. (5.7b) follows that whatever the core flow, there is no redistribution of the fluid in the y-direction in layers *P3, P4*. On the contrary, in layers *P5* and *P6* the y-component of the local flow rate is always non-zero unless $\widetilde{T} = 0$ at $z = \pm d$.

Consider now further particular cases. If temperature is ***independent of both z and x***, i.e. $\widetilde{T} = \widetilde{T}(y)$, then all the core flow variables, except for $j_{x,C}$, w_C, vanish, the latter being

$$w_C = \widetilde{T}\,. \tag{5.9}$$

In particular, for $\widetilde{T} = y$ (differentially heated Hartmann walls $y = \pm 1$; all other walls being thermally insulating), one gets:

$$j_{x,C} = -y\,, \; w_C = y\,. \tag{5.10}$$

The core current, induced in the negative and positive y-direction for $y > 0$ and $y < 0$, respectively (Fig. 2), shortcuts in the perfectly conducting walls 3 and 4 in the same cross-section z = constant, which is schematically shown with broken lines in Fig. 2.

There are no jets in layers P3, P4. Thus the flow in the bulk of the box is fully developed irrespective of the aspect ratio. The fluid simply ascends or descends in the core where $\widetilde{T}$ is positive or negative, respectively. At $z = \pm d$ the fluid turns in layers *P5* and *P6* in high-velocity jets. Consider layer *P5*, for example. For $\widetilde{T} = y$ local flow rates for this layer are given by the following expressions:

$$q_{x,5} = 0, \quad q_{y,5} = \tfrac{1}{2}(y^2 - 1). \tag{5.11}$$

Thus the fluid, which enters layer *P5* at the top of the box for $y > 0$ flows in the $-y$-direction and then descends in the core in a symmetric way. A schematic diagram of such a flow is shown in Fig. 2. As there is no flow in the x-direction in the layer, the flow is two-dimensional, in the (x,z)-planes, similar to that discussed by Garandet, Alboussière & Moreau (1992).

If temperature is ***independent of z***, i.e. $\widetilde{T} = \widetilde{T}(x, y)$, both y- and x- components of velocity vanish, and fluid ascends or descends in both the core and layers *P3, P4*. As the core potential evaluated at walls 3 and 4 is in general not equal to zero, from Eq. (5.7a) follows that *jets are present in layers P3, P4*. As follows from Eqs. (5.2), (5.7) and (5.9), locally the direction of the flow in the jets may not be the same as that in the adjacent core.

As an example consider the flow for $\widetilde{T} = xy$ (heating/cooling of the vertical walls with maxima and minima of temperature at the ribs $y = \pm 1$, $x = \pm l$, Fig. 3). The core variables are:

$$\phi_C = \tfrac{1}{6} y(1 - y^2), \quad j_{x,C} = -xy, \quad j_{z,C} = 0, \quad j_{y,C} = -\tfrac{1}{6} + \tfrac{1}{2} y^2, \tag{5.12}$$

$$\Psi_C = \tfrac{1}{2} x\left(y^2 - \tfrac{1}{3}\right), \quad u_C = 0, \quad v_C = 0, \quad w_C = xy, \tag{5.13}$$

$$q_{z,3,4} = \pm \tfrac{1}{6} y(1 - y^2), \quad q_{y,3,4} = 0, \tag{5.14}$$

$$q_{x,5,6} = \mp \tfrac{1}{6} y(1 - y^2), \quad q_{y,5,6} = \pm \tfrac{1}{2} x(y^2 - 1). \tag{5.15}$$

We observe that: (i) the core current has two components; the loops of current are shown in Fig. 4; (ii) apart from the vicinity of walls 5 and 6 the flow is fully developed; (iii) in layers *P5* and *P6* both components of local flow rates are non-zero (Fig. 5).

As there is a volume flux into layer *P5* from the core, vector lines for the local flow rate in layer *P5*, shown in Fig. 5, cannot be considered the streamlines. Once the fluid from the core enters layer *P5* for certain values of x and y, it follows these vector lines and finally leaves the layer back to the core in a symmetric way.

If temperature is ***independent of x***, i.e. $\widetilde{T} = \widetilde{T}(y, z)$ then w_C and $j_{x,C}$ are given by expressions (5.1a) and (5.9). All other core variables, except for v_C (given by Eq. (3.58)), vanish. The current loops are as those described for $\widetilde{T} = \widetilde{T}(y)$. As the core velocity now

involves the second component, v_C, the flow in the core occurs in the (y,z)-planes, i.e. exactly transverse to the core current. It is obviously no longer fully developed in the whole box. In addition, *there are no jets in layers P3, P4*.

It should be noted that for $\widetilde{T} = \widetilde{T}(y,z)$ and for $\widetilde{T} = 0$ at $z = \pm d$ (fixed, constant temperature at the top and bottom walls), jets in all the parallel layers vanish (cf. Eqs. (5.7), (5.8)). The fluid simply recirculates in the core in the planes x = constant. An example of such a temperature distribution is $\widetilde{T} = y(d^2 - z^2)$, which yields:

$$v_C = z(y^2 - 1), \quad w_C = y(d^2 - z^2).$$

The streamlines for this flow for $d = 1$ are shown in Fig. 6.

5.1.2 Perfectly conducting walls 1, 2; walls 3-6 - finite conductors

Now suppose that walls 1 and 2 are perfectly conducting, i.e. $\phi_1 = \phi_2 = 0$, while parallel walls 3-6 being of finite conductivity. Then potentials of walls 3-6 obey the following equations:

$$c_{3,4}\nabla^2_{yz}\phi_{3,4} = \pm\widetilde{T}(\pm l, y, z), \tag{5.16}$$

$$c_{5,6}\nabla^2_{xy}\phi_{5,6} = 0. \tag{5.17}$$

subject to boundary conditions (3.51) and

$$\phi_{3\text{-}6} = 0 \quad \text{at } y = \pm 1. \tag{5.18}$$

It should be noted that the problem for wall potentials $\phi_{3\text{-}6}$ may be solved analytically in terms of Fourier series.

Taking into account y-symmetry of the problem, the y-components of the local flow rates carried by layers *P3-P6* become:

$$q_{y,3,4}(y,z) = \pm\int_{-1}^{y}\frac{\partial\phi_{3,4}}{\partial z}dy, \quad q_{y,5,6} = \mp\int_{-1}^{y}\left[\widetilde{T}(x,t,\pm d) - \frac{\partial\phi_{5,6}}{\partial x}\right]dt, \tag{5.19}$$

while those transverse to the field are given by Eqs. (3.61) and (3.63).

It follows that while the core flow is exactly the same as for all walls being perfect conductors, jets in parallel layers *P3* and *P4* are present. Thus the flow in parallel layers is three-dimensional even if temperature is independent of x or z.

There is one exception to the above flow pattern, namely for $\widetilde{T}(\pm l, y, z) = 0$, i.e. for a fixed, constant temperature of walls 3 and 4. In this case potentials of walls 3-6 vanish irrespective of the values of their wall conductance ratios. The reason for this is that there is no normal component of core current to the parallel walls. An example of such a temperature distribution is $\widetilde{T} = y(l^2 - x^2)$ (Fig. 7). In this case,

$$j_{x,C} = y(x^2 - l^2)\,, \quad j_{y,C} = x(\tfrac{1}{3} - y^2)\,, \quad \Psi_C = \tfrac{1}{2} y^2 (l^2 - x^2) + \tfrac{1}{6} x^2\,. \tag{5.20}$$

The core current, shown in Fig. 8, shortcuts via perfectly conducting Hartmann walls. Thus there is no "need" for the current to pass through the parallel walls, which thus remain passive.

5.1.3 Perfectly conducting walls 3-6; walls 1 and 2 - finite conductors

If walls 3-6 are perfectly conducting, then potentials ϕ_3-ϕ_6 vanish. For an odd temperature with respect to y, and for $c_2 = c_1$ one gets $\phi_2 = -\phi_1$, while the problem governing potential ϕ_1 becomes:

$$c_1 \nabla^2_{xz} \phi_1 - \phi_1 = -\int_0^1 y \frac{\partial \widetilde{T}}{\partial x}\, dy\,, \tag{5.21}$$

$$\phi_1 = 0 \quad \text{at } x = \pm l, \tag{5.22}$$

$$\phi_1 = 0 \quad \text{at } z = \pm d. \tag{5.23}$$

It should be noted that the solution to this problem may be obtained analytically in terms of Fourier series for an arbitrary temperature distribution.

The core variables are given by equations:

$$\phi_C = y\phi_1 + y\widetilde{M}_x(x,1,z) - \widetilde{M}_x(x,y,z)\,, \tag{5.24}$$

$$j_{y,C} = -\phi_1 - \widetilde{M}_x(x,1,z) + \int_0^y \frac{\partial \widetilde{T}}{\partial x}(x,t,z)\, dt\,, \tag{5.25}$$

$$u_C = \frac{\partial \phi_C}{\partial z}\,, \quad w_C = \widetilde{T} - \frac{\partial \phi_C}{\partial x}\,. \tag{5.26}$$

Compared to Sec. 5.1.1 there are new terms involving ϕ_1 in Eqs. (5.24) and (5.25). They are related to the additional current flowing in the y-direction owing to the difference of potentials of walls 1 and 2.

However, if temperature is ***independent of x***, from Eqs. (5.21)-(5.23) follows that $\phi_1 = 0$, so that the flow becomes exactly the same as that for all walls being perfect conductors. This holds, for example, for $\widetilde{T} = y$ (the case of differentially heated Hartmann walls, discussed in Sec. 5.1.1). The reason is that the core current enters neither wall 1 nor 2 (cf. Fig. 2). It shortcuts in walls 3 and 4 between $y > 0$ and $y < 0$ in the same cross-section z = constant.

If temperature ***varies with x***, the are two possibilities. The **first** one is that the expression

$$\widetilde{m}_x = -\int_0^1 y \frac{\partial \widetilde{T}}{\partial x} dy \qquad (5.27)$$

vanishes. Then ϕ_1 vanishes as well, and the core flow is again exactly the same as for perfectly conducting walls.

The expression (5.27) represents the *y*-component of the temperature-driven current entering the Hartmann walls. Even if such a current is induced in the core, but it does not enter the Hartmann walls, the latter again remain passive. An example of such a flow occurs for $\widetilde{T} = xy(1-\frac{5}{3}y^2)$ (Fig. 9). In this case

$$j_{x,C} = -xy(1-\tfrac{5}{3}y^2), \quad j_{y,C} = \tfrac{1}{12}(-1+6y^2-5y^4), \quad \Psi_C = \tfrac{1}{12}x(-1+6y^2-5y^4). \qquad (5.28)$$

The lines of core current are shown in Fig. 10.

Even if c_1 and c_2 are arbitrary, not equal to each other, but $\widetilde{m}_x = 0$, then the flow will still be anti-symmetric with respect to *y*. Indeed, from Eqs. (3.47), (3.52), (3.53) follows that for *y*-anti-symmetric temperature and perfectly conducting parallel walls the core pressure vanishes even if $c_1 \neq c_2$, and thus cannot affect the core flow. Further, if $\widetilde{m}_x = 0$ functions ϕ_1 and ϕ_2 obey homogeneous Eqs. (3.48) subject to boundary conditions

$$\phi_{1,2} = 0 \quad \text{at } x = \pm l \text{ and at } z = \pm d. \qquad (5.29)$$

The solution to the problem is trivial, namely

$$\phi_{1,2} = 0. \qquad (5.30)$$

Thus conductance of walls 1 and 2 plays no role, i.e. they behave as if they were perfectly conducting.

The **second** possibility is that expression (5.27) is non-zero. Then the whole core flow will be affected by the finite conductance of the Hartmann walls. This will happen, for example for current closure patterns shown in Figs. 4 and 8. In this case jets in layers *P3* and *P4* are always present.

Finally we note that the flow discussed in this section has many similarities with that in an insulating rectangular box in a vertical magnetic field considered by Aleksandrova (2001). In that problem, however, jets in the parallel layers were of much higher magnitude, namely *O*(*Ha*).

5.1.4 All walls of finite conductance

Suppose now that all the walls have a finite electrical conductance. Now conductance ratios of all walls will affect the flow pattern unless normal component of the core current vanishes at all the boundaries of the box. The latter situation occurs if and only if

$$\widetilde{T} = 0 \quad \text{at } x = \pm l, \qquad (5.31)$$

and $$\widetilde{m}_x = 0\,. \tag{5.32}$$

For the sake of simplicity we further assume that one of the conditions (5.31) or (5.32) is not fulfilled and that all the walls have the same walls conductance ratio, i.e. $c_i = c$ for $i = 1,\ldots,6$. Then owing to symmetry one gets $\phi_2 = -\phi_1$, $\phi_4 = -\phi_3$, $\phi_6 = \phi_5$.

Consider the case of differentially heated Hartmann walls, i.e. $\widetilde{T} = y$, discussed in Sec. 5.1.1. Then the equations governing electric potentials of walls 1, 3, 5 are:

$$c\nabla^2_{xz}\phi_1 - \phi_1 = 0\,, \tag{5.33}$$

$$c\nabla^2_{yz}\phi_3 = y\,, \tag{5.34}$$

$$\nabla^2_{xy}\phi_5 = 0\,. \tag{5.35}$$

The flow is symmetric with respect to both x and z, which leads to the following conditions:

$$\phi_1 = 0\,, \quad \phi_5 = 0 \quad \text{at } x = 0, \tag{5.36}$$

$$\phi_3 = 0\,, \quad \phi_5 = 0 \quad \text{at } y = 0, \tag{5.37}$$

$$\partial\phi_1/\partial z = 0\,, \quad \partial\phi_3/\partial z = 0 \quad \text{at } z = 0. \tag{5.38}$$

The expressions for the core variables become:

$$\phi_C = y\phi_1\,, \tag{5.39}$$

$$j_{x,C} = -y\,, \quad j_{y,C} = -\phi_1\,, \quad j_{z,C} = 0\,, \tag{5.40a-c}$$

$$u_C = y\frac{\partial\phi_1}{\partial z}\,, \quad v_C = 0\,, \quad w_C = y - y\frac{\partial\phi_1}{\partial x}\,. \tag{5.41a-c}$$

From Fig. 2 one might conclude that the closure pattern of the electric current indicates that only walls 3 and 4 would be active. This is not the case, however. The primary, $x-$ component of current driven by temperature, is given by Eq. (5.40a), which is the same as for perfectly conducting walls. This current creates differences in the electric potential along both walls 3 and 4, which drive wall currents along these walls in the positive and negative $y-$direction, respectively. However, as a result of this, potential difference is created between corners of the z = constant cross-section of the box, namely $x = -l$, $y = 1$ and $x = -l$, $y = 1$. This leads to the variation of the potential of wall 1. Owing to symmetry, the same in magnitude but the opposite in sign potential difference is created between the other two corners, namely $x = -l$, $y = -1$ and $x = -l$, $y = -1$. This leads to variation of function ϕ_2 (= $-\phi_1$). The resulting core potential (Eq. (5.39)) drives the y-component of the core current (Eq. (5.40b)). Thus the whole closure pattern of current is restructured. While it resembles that shown in Fig. 2, the core current may now enter/leave the Hartmann walls, which become active.

The results of numerical calculations for $\widetilde{T} = y$, $c = 0.1$, $l = 1$, $d = 5$ are shown in Figs. 11-16. As the box is sufficiently high, the flow near the centre-plane, $z = 0$, is close to being fully developed, i.e. independent of z (cf. Fig. 12 for potentials of walls 1 and 3, for example). Thus it is the same as for an infinitely long duct with the fluid flowing strictly along the z-axis. Such a flow has been studied analytically by Bühler (1998). It should be noted that the co-ordinate system in that study has a different orientation from that used here. The numerical method used here has been verified on an analytical solution presented by Bühler (1998). The results for potential ϕ_3, shown in Fig. 11, are in excellent agreement.

Consider first the fully developed flow region at $z = 0$. As has been mentioned before the core current passes through walls 1-4, creating potential difference along all these walls as shown in Fig. 13 (signs in circles). The difference in potentials of walls 1 and 2 results in the non-zero core potential, Eq. (5.39). Variation of this potential in the box cross-section affects the distribution of the vertical velocity via the second term in Eq. (5.41c). From Fig. 14 follows that the finite conductance of walls significantly affects the core flow. The maximum value of the core velocity, reacted at the corners $x = \pm 1$, $y = 1$ at $z = 0$ is 3.43 compared to the value of 1 for all walls being perfect conductors.

The reason why velocity becomes higher is this. If the Hartmann walls are perfect conductors, the core potential vanishes. It is a very well known fact that the flow in ducts with perfectly conducting walls is highly damped by a transverse magnetic field. If walls are finite conductors, Hartmann-wall potentials are no longer zero, leading to wall currents flowing in the opposite direction to those induced by buoyancy term in the core (Fig. 13). Thus the non-zero wall potentials, which drive these currents, tend to increase the core velocity. Note that for insulating walls such an increase in some cases may be by $O(Ha)$ (Aleksandrova (2001)).

As there is a difference between potentials of walls 3 and 4 and the values of the core potential estimated at $x = \pm 1$, there are jets at parallel walls 3 and 4. The z-component of the local flow rate for layer *P3* is shown in Fig. 15 (solid line).

Closer to the top of the box the flow is no longer fully developed. As $P = 0$, the flow restructures exclusively by the closure pattern of the electric current. Fig. 12 shows isolines of potentials of walls 1, 3 and 5 in the 1/8th of the box. The wall current flows transverse to these isolines. The core current, still being induced in the cross-section z = constant, thus enters walls 1-4 only. However, it may now turn in the z-direction and complete the circuit in wall 5 if such a path is shorter and by implication resistance lower. As a result, the induced core potential becomes a function of z. Thus the z-component of core velocity is modified (Fig. 14). As close to the top of the box potential differences become lower, then w_C decreases with increasing z for $y > 0$. The core looses fluid into parallel layers *P3* and *P4*, which is carried by the positive x-component of core velocity (Fig. 16).

Basically, at the top of the box the upward-moving fluid for $y > 0$ must turn and flow downwards for $y < 0$ in a symmetric way. For perfectly conducting walls this turning core

flow occurred strictly in the $-y$-direction in a layer *P5*. Such a path for the fluid will also remain for the present flow. The core velocity profile at the boundary with layer *P5* is shown in Fig. 14 for $z = 5$. From the magnitudes of core velocity at $z = 0$ and $z = 5$ follows that most of the core flow will follow this path. It should be noted that the turning of the flow in the $-y$-direction in the core is forbidden as $v_C = 0$.

As the walls here are finite conductors, jets in layers *P3* and *P4* are present. The flow in these jets must also turn in the $-y$-direction at the top. As a result the magnitudes of the $z-$components of the local flow rate in the layers decrease with increasing z. The fluid which was "lost" by the core owing to the x-component of core velocity also turns in the layers and reappears in the core for $y < 0$ in a symmetric way.

From Figs. 12, 14-16 follows that for the chosen values of c and of dimensions of the box all the three-dimensional effects are confined to about one value of characteristic length from the top (and the bottom).

Finally, the height of the box, d, has been varied to determine the minimum value of d for the fully developed flow to establish in the centre-plane, at $z = 0$. The results for the maximum vertical component of core velocity, shown in Fig. 17, indicate that the value of d of about 3 is sufficient.

5.2 *y*-symmetric case

If temperature is symmetric with respect to y and $c_1 = c_2$, then P, ϕ_C, $j_{x,C}$, w_C, u_C are symmetric, while $j_{y,C}$ and v_C are anti-symmetric. We note first that the core pressure is no longer zero, and thus the core current may have all three components. For $c_1 = c_2$ one gets $\phi_1 = \phi_2$, so that the core potential and y-component of current become:

$$\phi_C = \phi_1 + \hat{M}_x(x,1,z) - \hat{M}_x(x,y,z), \tag{5.42}$$

$$j_{y,C} = \int_0^y \frac{\partial \hat{T}}{\partial x}(x,t,z)dt\,. \tag{5.43}$$

It is seen that $j_{y,C}$ is directly expressed in terms of temperature.

Again, we start the investigation for a box with certain walls being perfect conductors.

5.2.1 All walls perfectly conducting

If all the walls are perfectly conducting, then wall potentials vanish, while the core flow now depends on temperature and pressure only. Once pressure is determined from Eq. (3.47) subject to boundary conditions

$$\frac{\partial P}{\partial x} = 0 \quad \text{at } x = \pm l, \tag{5.44}$$

$$\frac{\partial P}{\partial z} = \frac{1}{2}\int_{-1}^{1} T dy \quad \text{at } z = \pm d, \tag{5.45}$$

the core flow becomes fully defined. It should be noted that the problem for core pressure may be solved analytically in terms of Fourier series.

The expressions for the local flow rates in layers *P3-P6* are:

$$q_{z,3,4}(y,z) = \pm\phi_C(x = \pm l), \quad q_{y,3,4}(y,z) = 0, \tag{5.46a,b}$$

$$q_{x,5,6}(x,y) = \mp\phi_C(z = \pm d), \quad q_{y,5,6} = \pm\int_{-1}^{y}\hat{T}(x,t,\pm d)dt \mp \frac{1}{2}(y+1)\int_{-1}^{1}\hat{T}(x,t,\pm d)dt. \tag{5.47a,b}$$

As for the *y*-anti-symmetric temperature, there is no redistribution of the flow in the *y*-direction in layers *P3, P4*.

Consider now particular cases. If temperature is ***independent of both z and x***, i.e. $\hat{T} = \hat{T}(y)$, then the solution for the core pressure is:

$$P = kz, \tag{5.48}$$

where $k = \frac{1}{2}\int_{-1}^{1}\hat{T}dy = \text{constant}$ is the pressure gradient, which equals average temperature.

The core variables become:

$$\phi_C = 0, \quad j_{x,C} = k - \hat{T}, \quad j_{y,C} = 0, \quad j_{z,C} = 0, \tag{5.49a-d}$$

$$u_C = 0, \quad v_C = 0, \quad w_C = \hat{T} - k. \tag{5.50a-c}$$

From the above expressions follows that the current is induced in the *x*-direction only, while the core flow is strictly vertical.

As the total current vanishes, the current induced in the *x*-direction in the cross-section *z* = constant, shortcuts in the walls 3 and 4, and returns in the –*x*-direction in the same cross-section. Concerning velocity, there is an upward motion if temperature is higher than average, and downward one if it is lower than average.

There are no jets in layers *P3* or *P4*. In layers *P5*, *P6* the fluid flows along the *y*-axis only.

An example of such a flow for $\hat{T} = \frac{1}{2}(1-y^2)$, i.e. for uniform volumetric heating $Q = 1$, $\hat{T} = 0$ at the Hartmann walls, and all other walls being thermally insulating, is shown in Fig. 18. In this case, $k = 1/3$, $w_C = -j_{x,C} = \frac{1}{2}(\frac{1}{3} - y^2)$, $q_{y,5,6} = \pm\frac{1}{6}y(1-y^2)$. In the core the fluid flows upwards in the centre and downwards at the Hartmann walls. When upward-

moving fluid enters layer *P5*, it is redistributed towards the Hartmann walls in the $\pm y$ direction.

If temperature is ***independent of z***, i.e. $\hat{T} = \hat{T}(x, y)$, the y-component of velocity and the source term in equation (3.47) for the core pressure vanish. However, in contrast to the y–anti-symmetric temperature, the x-component of velocity is non-zero as it depends on core pressure. Thus in the core the flow is in the planes y = constant.

If temperature is ***independent of x***, i.e. $\hat{T} = \hat{T}(y, z)$ then Eqs. (5.49), (5.50a,c) still hold, while v_C is given by expression (3.59). All other core variables vanish. The current loops are as those described for $\widetilde{T} = \widetilde{T}(y)$. As the core velocity now involves the second component, v_C, the flow in the core occurs in the (y,z)-planes, i.e. exactly transverse to the core current. It is no longer fully developed in the whole box.

For either walls 1, 2, or walls 3-6 being perfect conductors, while the other walls of finite conductivity, the analysis is similar to that for y-anti-symmetric temperature. In particular, if $c_i \to \infty$, then walls 1 and 2 become passive if the net heat flux

$$\hat{m}_x = \int_0^1 \frac{\partial \hat{T}}{\partial x} dy \tag{5.51}$$

vanishes.

5.2.2 All walls of finite conductance

In this section two examples of flows owing to the y-symmetric temperature distribution will be considered. Supposed that the fluid is heated with uniform distribution of volumetric heat sources, i.e. Q = 1, and that the dimensionless temperature of either the Hartmann walls or walls 3 and 4 is zero, while all other walls are thermally insulating. This leads to two different temperature distributions as follows: (i) $\hat{T} = \frac{1}{2}(1 - y^2)$ and (ii) $\hat{T} = \frac{1}{2}(l^2 - x^2)$, respectively.

Case (i): $\hat{T} = \frac{1}{2}(1 - y^2)$

The flow in a box with perfectly conducting walls owing to this temperature distribution has been studied in Sec. 5.2.1. Now suppose, for the sake of simplicity, that $c_i = c < \infty$ (i=1,…,6), i.e. that all walls have the same, finite wall conductance ratio. Owing to symmetry $\phi_2 = \phi_1$, $\phi_4 = -\phi_3$, $\phi_6 = \phi_5$. Then the equations governing electric potentials of walls 1, 3, 5 and pressure are:

$$\nabla^2_{xz} \phi_1 = 0, \tag{5.52}$$

$$c\nabla^2_{yz}\phi_3 = -\left.\frac{\partial P}{\partial z}\right|_{x=l} + \frac{1}{2}(1-y^2), \tag{5.53}$$

$$c\nabla^2_{xy}\phi_5 = \left.\frac{\partial P}{\partial x}\right|_{z=d}, \tag{5.54}$$

$$\nabla^2_{xz} P = 0. \tag{5.55}$$

These equations are solved subject to boundary conditions (3.51)-(3.53) and the following symmetry conditions:

$$\phi_1 = 0, \quad \phi_5 = 0, \quad \partial P/\partial x = 0 \quad \text{at } x = 0, \tag{5.56}$$

$$\partial\phi_3/\partial y = 0, \quad \partial\phi_5/\partial y = 0 \quad \text{at } y = 0, \tag{5.57}$$

$$\partial\phi_1/\partial z = 0, \quad \partial\phi_3/\partial z = 0, \quad P = 0 \quad \text{at } z = 0. \tag{5.58}$$

The core variables become:

$$\phi_C = \phi_1, \tag{5.59}$$

$$j_{x,C} = -\frac{1}{2}(1-y^2) + \frac{\partial P}{\partial z}, \quad j_{y,C} = 0, \quad j_{z,C} = -\frac{\partial P}{\partial x}, \tag{5.60a-c}$$

$$u_C = \frac{\partial\phi_1}{\partial z} - \frac{\partial P}{\partial x}, \quad v_C = 0, \quad w_C = \frac{1}{2}(1-y^2) - \frac{\partial\phi_1}{\partial x} - \frac{\partial P}{\partial z}. \tag{5.61a-c}$$

The core current now has two components, x and z. As y-component of current is zero, close to the centre-plane $z = 0$ the current may enter/leave walls 3 or 4 only. Further it selects a path to complete its circuit either inside walls 3 or 4, or between walls 3 and 4 through walls 1 or 2. Inside the walls the current flows transverse to the isolines of wall potential shown in Fig. 19. At the top of the box wall 5 is also involved in the current closure pattern.

The vertical velocity component depends now on the wall potential ϕ_1 (Eq. (5.61c)), and thus is a function of all the three co-ordinates (Fig. 20). The velocity profile at $z = 0$, shown in Fig. 20, looks similar to that for a box with perfectly conducting walls. However, it is shifted downwards compared to the profile presented in Fig. 18. The reason is that almost the entire volume flux in the z-direction is now carried by jets in layers *P3* and *P4* (Fig. 21). In fact, vertical component of velocity in the core is negative almost in the whole cross-section apart from immediate vicinity of the centre-plane $y = 0$, where it reaches a value of approximately 0.01.

As for a box with perfectly conducting walls, vertical pressure gradient is induced as described at the end of Sec. 2. Now, however, it depends on the wall conductance ratio, and thus differs from the value of 1/3 for perfectly conducting walls.

At the top of the box potential ϕ_3 starts varying with z, and this induces the pressure gradient in the x-direction (cf. Eq. (3.51)). As a result the z-component of current appears. The results show, however, that the transverse pressure difference between $x = 0$ and $x = 1$ is very small and is confined to the immediate vicinity of the top of the box.

At the top of the box the fluid must turn from the upward flow in layers *P3*, *P4* into the downward one in the core. This happens both in layer *P5* and the core owing to the x–component of velocity. The second path is possible in the core owing to a non-zero x–component of velocity. From Fig. 19 follows that the three-dimensional effects are confined to about one value of the characteristic length at the top of the box.

Case (ii): $\hat{T} = \frac{1}{2}(l^2 - x^2)$

The fully developed flow under such conditions has been discussed by Bühler (1998). Note that in that paper temperature at the centre, at $x = 0$, denoted by Θ was chosen to such a value that the pressure gradient evaluates to zero. That approach was guided by the idea that it is possible to chose the reference temperature T_0^* to such a value that the hydrostatic pressure gradient $-\rho_0^* T_0^* g^*$ in the Boussinesq approximation balances the pressure gradient induced by the flow.

For the temperature distribution (ii), and for all walls having the same wall conductance ratio, the same symmetry conditions for wall potentials and pressure hold as for (i). Thus the only difference is in the equations for ϕ_1 and ϕ_3, namely:

$$c\nabla_{xz}^2 \phi_1 = x\,, \tag{5.62}$$

$$c\nabla_{yz}^2 \phi_3 = -\left.\frac{\partial P}{\partial z}\right|_{x=l}\,. \tag{5.63}$$

The core variables become:

$$\phi_C = \phi_1 + \tfrac{1}{2}x(y^2 - 1)\,, \tag{5.64}$$

$$j_{x,C} = -\tfrac{1}{2}(x^2 - l^2) + \frac{\partial P}{\partial z}\,, \quad j_{y,C} = -xy\,, \quad j_{z,C} = -\frac{\partial P}{\partial x}\,, \tag{5.65a-c}$$

$$u_C = \frac{\partial \phi_1}{\partial z} - \frac{\partial P}{\partial x}\,, \quad v_C = 0\,, \quad w_C = \tfrac{1}{2}(l^2 - x^2 + 1 - y^2) - \frac{\partial \phi_1}{\partial x} - \frac{\partial P}{\partial z}\,. \tag{5.66a-c}$$

The core current now has all three components. In the fully developed region, however, the z-component of current vanishes, so that the current flows in the (x,y)-planes. Once current enters walls, it flows transverse to the isolines of wall potential shown in Fig. 22.

Vertical velocity component also depends on all three co-ordinates (Fig. 23). The velocity profile at $z = 0$, shown in Fig. 23, looks similar to that presented by Bühler (1998) for

a box with perfectly conducting walls. However, the magnitude of velocity is higher. The buoyancy-induced contribution into w_C, given by the first term in Eq. (5.66c) has a maximum value of 0.5 compared to the maximum value of 4 in Fig. 23. Thus, the flow at these values of parameters, c, l, and d, is mainly electrically driven. In the core the fluid flows upwards at the centre plane $x = 0$ and downwards at walls $x = \pm l$. At walls 3 and 4 downward jets are present (Fig. 24). Again, this is similar to the results presented by Bühler (1998).

At the top of the box the induced pressure starts varying with x owing to variation of ϕ_3 with z. Thus the pressure gradient in the x-direction is induced (Fig. 24). As a result the z–component of current appears.

At the top of the box the fluid must turn from the upward flow in the core at $x = 0$ into the downward one at $x = \pm 1$ in both core and layers *P3*, *P4*. This happens both in layer *P5* and the core owing to the x-component of velocity. From Figs. 22 and 24 follows that the three-dimensional effects are confined to about one value of the characteristic length at the top of the box.

6 Conclusions

Buoyant convection in a rectangular box with thin electrically conducting walls in the presence of a strong, uniform, horizontal magnetic field has been considered. The temperature, which drives this convective flow was supposed to be an arbitrary function of all the three co-ordinates. This includes such practically important cases as differentially heated walls and volumetric heat sources.

The driving mechanism of the flow is buoyancy. Variation of temperature leads to buoyancy force leading to the ascending fluid in some parts of the box and descending in the other ones. Once fluid starts moving in a transverse field, electric currents are induced in the flow. The current induced by buoyant motion creates potential gradients in the fluid and along various walls. Induced potentials along the Hartmann walls serve as boundary values for the solution in the core and thus restructure both the core current closure pattern and the velocity profiles. Thus the resulting flow patterns are created not only by purely thermal buoyancy. They are a result of all mechanisms involved, i.e. buoyant-, viscous- and electromagnetic-forces. The latter ones depend on current magnitude and path which is very sensitive to the conductivity of the walls.

In addition to this, jets with velocities on the order $O(Ha^{1/2})$ may be present in the parallel layers. In the jets the component of high velocity transverse to the field is created by the strong gradients of the electric potential normal to the layer. The flow rate carried by the layer in this direction is related to the jump of potential across the layer between the wall and the core. Therefore, jets may or may not vanish depending on whether such jumps exist. There

exist certain distributions of temperature which may exclude jets in parallel layers if the induced current is tangential to all the walls, even if these walls are poorly conducting.

This and ultimately the whole flow pattern strongly depends on the following conditions: (i) symmetries of temperature with respect to all the three co-ordinates, (ii) the type of thermal boundary conditions at the walls parallel to the magnetic field, (iv) average heat fluxes in the x- and z-direction, (iii) the values of wall conductance ratios. The flow turns out to be sensitive to any variation of the above conditions.

Finally, we note that the numerical code developed to model buoyant convective flows in a rectangular box for arbitrary conductance ratios of all the walls is a fast, flexible tool, which may be efficiently used to analyse and optimise convective flows in liquid metal blankets.

7 Acknowledgement

This work has been performed within the framework of the Nuclear Fusion Program of the Forschungszentrum Karlsruhe in collaboration with Coventry University and is supported by the European Union within the European Fusion Technology Program TW1-TTBA-006 D2.

8 References

T. Alboussière, J. P. Garandet and R. Moreau, "Buoyancy-driven convection with a uniform magnetic field. Part 1. Asymptotic analysis," *J. Fluid Mech.* **253**, 545-563 (1993).

T. Alboussière, J. P. Garandet and R. Moreau, "Asymptotic analysis and symmetry in MHD convection," *Phys. Fluids* **8**, 2215-2226 (1996).

S. Aleksandrova, "Buoyant convection in cavities in a strong magnetic field," *PhD Thesis, Coventry University* (2001).

S. Aleksandrova and S. Molokov, "Classification of buoyant convective flows in cylindrical cavities in a strong, uniform, axial magnetic field," *Proc. 5th Intern. PAMIR Conf. on Fundamental and Applied MHD, Ramatuelle, France, Sept. 16-20, 2002*, I-81 – I-86 (2002).

H. Ben Hadid, D. Henry and S. Kaddeche, "Numerical study of convection in the horizontal Bridgman configuration under the action of a constant magnetic field. Part 1. Two-dimensional flow," *J. Fluid Mech.* **333**, 23-56 (1997).

H. Ben Hadid and D. Henry, "Numerical study of convection in the horizontal Bridgman configuration under the action of a constant magnetic field. Part 2. Three-dimensional flow," *J. Fluid Mech.* **333**, 57-83 (1997).

V. Bojarevics, "Buoyancy driven flow and its stability in a horizontal rectangular channel with an arbitrary oriented transversal magnetic field," *Magnetohydrodynamics* **31**, 245-253 (1995).

L. Bühler, "Laminar buoyant magnetohydrodynamic flow in vertical rectangular ducts," *Phys. Fluids* **10**, 223-236 (1998).

I. Di Piazza and L. Bühler, "Numerical simulations of buoyant magnetohydrodynamic flows using the CFX code," *Forschungszentrum Karlsruhe Report, FZKA 6354* (1999).

M. A. Fütterer, L. Barleon, L. Giancarli, A. Li Puma, O.V. Ogorodnikova, Y. Poitevin, J.F. Salavy, J. Szczepanski, G. Vella, "Potential and limits of water-cooled Pb-17Li blankets and divertors for a fusion power plant", *Fusion Engineering and Design* **49-50**, 543-549 (2000)

G. P. Garandet, T. Alboussière and R. Moreau, “Buoyancy driven convection in a rectangular enclosure with a transverse magnetic field,” *Int. J. Heat Mass Transfer* **35**, 741-748 (1992).

L. Giancarli, Y. Severi, L. Baraer, P. Leroy, J. Mercier, E. Proust, and J. Quintric-Bossy, “Water-cooled lithium-lead blanket design studies for demo reactor: Definition and recent developments of the box-shaped concept”, *Fusion Technology* **21**, 2081-2088 (1992).

L. N. Hjellming and J.S. Walker, “Melt motion in a Czochralski crystal puller with an axial magnetic field: motion due to buoyancy and thermocapillarity,” J. Fluid Mech. **182**, 335-368 (1987).

T.Q. Hua, J.S. Walker, B.F. Picologlou, and C.B. Reed, “Three-dimensional magneto-hydrodynamic flows in rectangular ducts of liquid-metal-cooled blankets,” *Fusion Technology* **14**, 1389-1398 (1998).

N. Ma and J.S. Walker, ”Liquid-metal buoyant convection in a vertical cylinder with a strong vertical magnetic field and with a nonaxisymmetric temperature,” *Phys. Fluids* **7**, 2061-2071 (1995).

S. Molokov and L. Bühler, “Numerical simulation of liquid-metal flows in radial-toroidal-radial bends,” *Kernforschungszentrum Karlsruhe Report, KfK-5160* (1993).

S. Molokov and L. Bühler, “Liquid-metal flow in a U-bend in a strong uniform magnetic field,” *J. Fluid Mech.* **267**, 325-352 (1994).

H. Ozoe and K. Okada, “The effect of the direction of the external magnetic field on the three-dimensional natural convection in a cubical enclosure,” *Int. J. Heat Mass Transfer* **32**, 1939-1954 (1989).

K. Okada and H. Ozoe, “Experimental heat transfer rates of natural convection of molten gallium suppressed under an external magnetic field in either the x, y, or z direction,” *Trans. ASME: J. Heat Transfer* **114**, 107-114 (1992).

T. Tagawa and H. Ozoe, “Enhancement of heat transfer rate by application of a static magnetic field during natural convection of liquid metal in a cube,” *Trans. ASME: J. Heat Transf.* **119**, 265-271 (1997).

T. Tagawa and H. Ozoe, “The natural convection of a liquid metal in a cubical enclosure with various electroconductivities of the wall under the magnetic field,” *Int. J. Heat Mass Transfer* **41**, 1917-1928 (1998).

J.S. Walker, “Models of melt motion, heat transfer and mass transport during crystal growth with strong magnetic fields,” *Progr. Crystal Growth and Characterization of Materials,* 195-213 (1999).

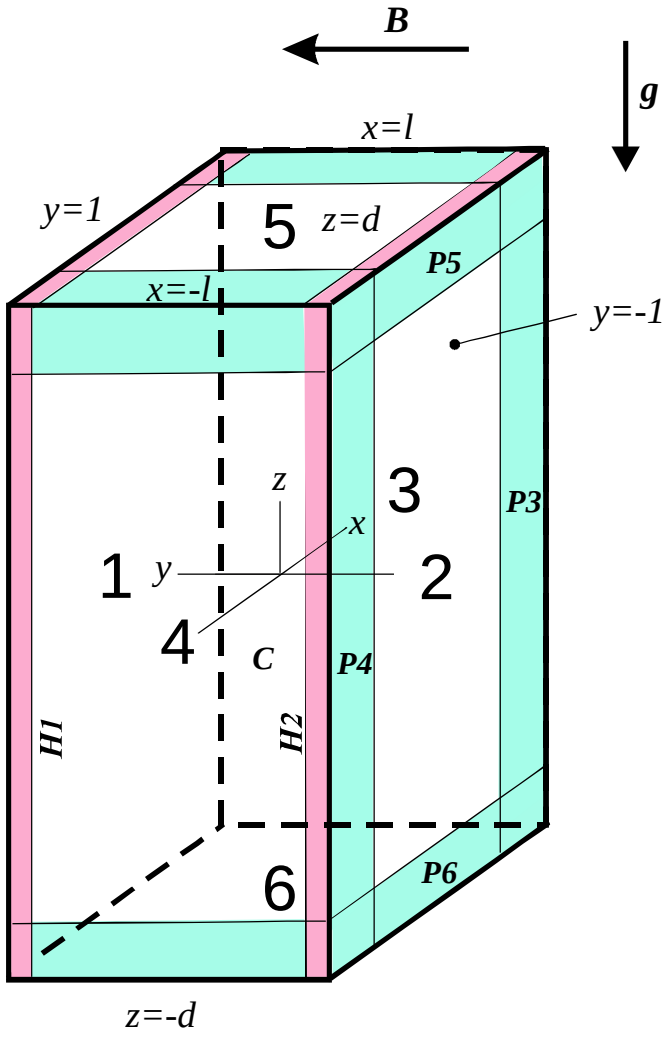

Fig. 1 Schematic diagram of the flow domain and flow subregions for high *Ha*

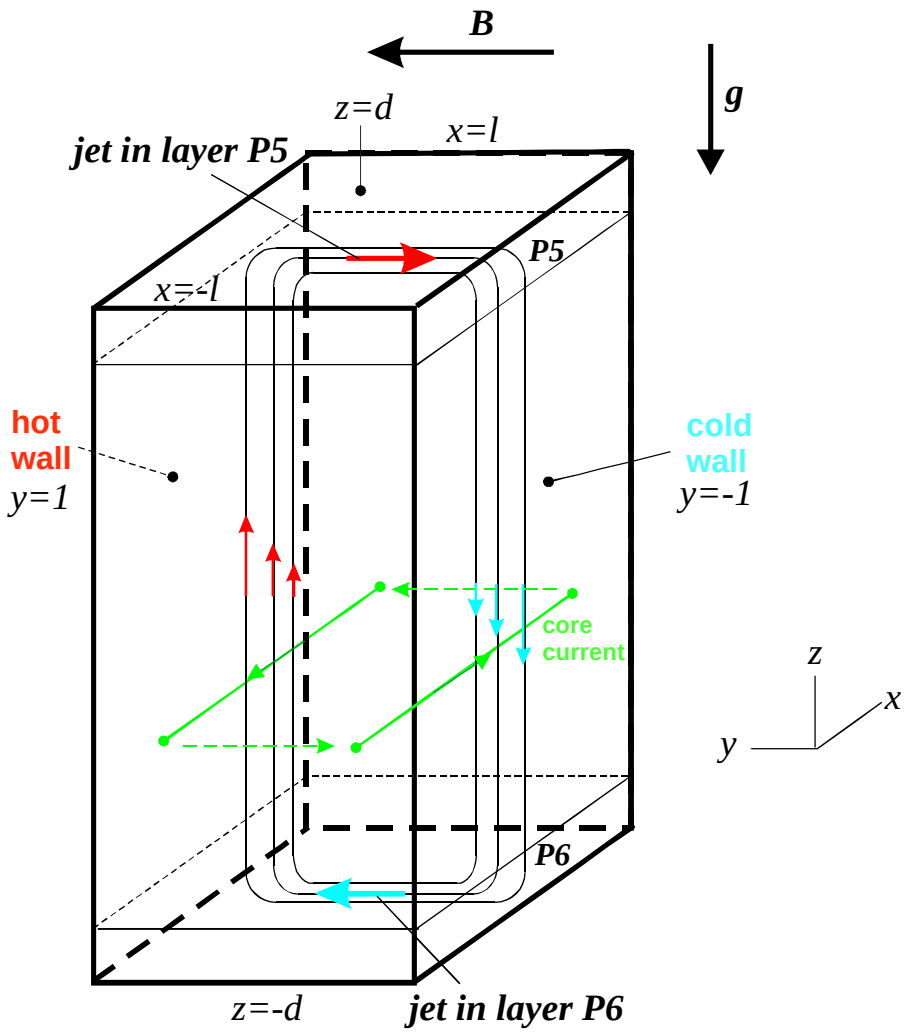

Fig. 2 Schematic diagram of the flow for perfectly conducting walls and for $T = y$: streamlines (black) and core current (green arrows). Ascending and descending flow is shown with red and blue arrows, respectively. Core current shortcuts via parallel walls in a way shown with broken green lines.

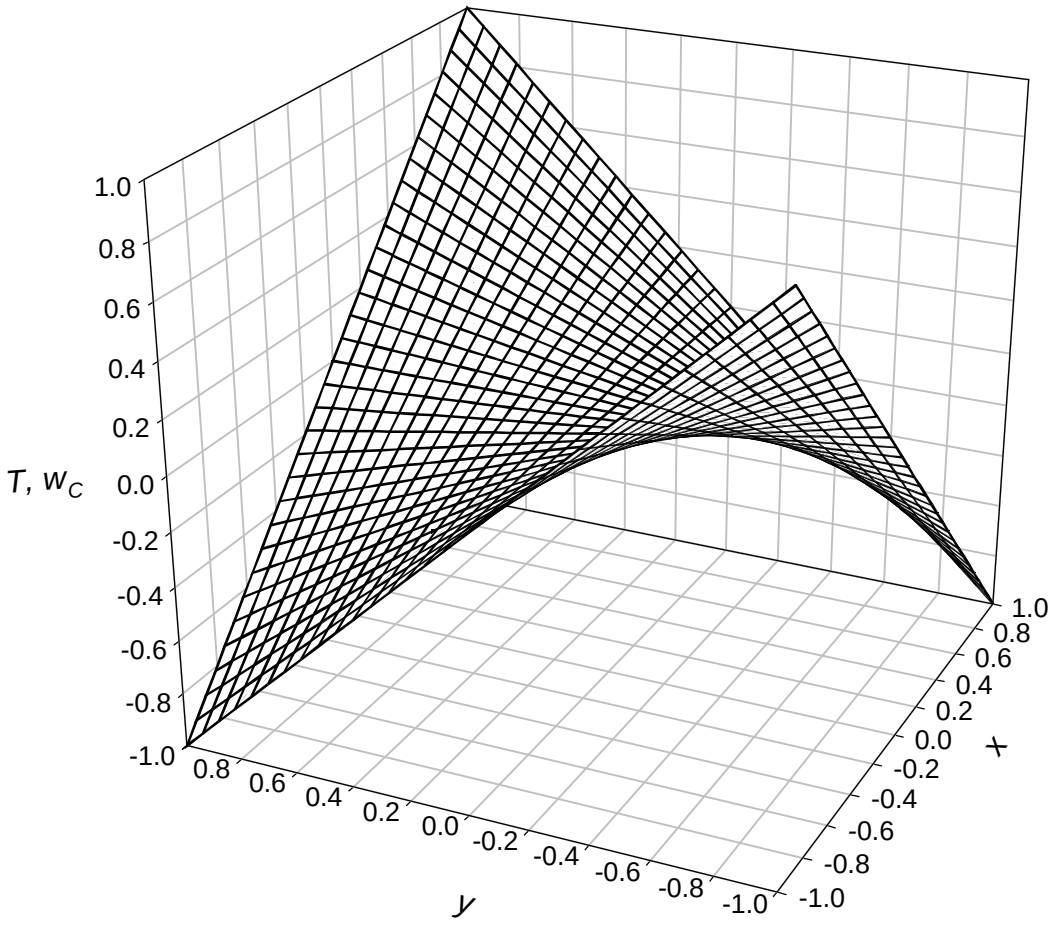

Fig. 3 Temperature $T = xy$ and vertical component of core velocity. All walls are perfectly conducting.

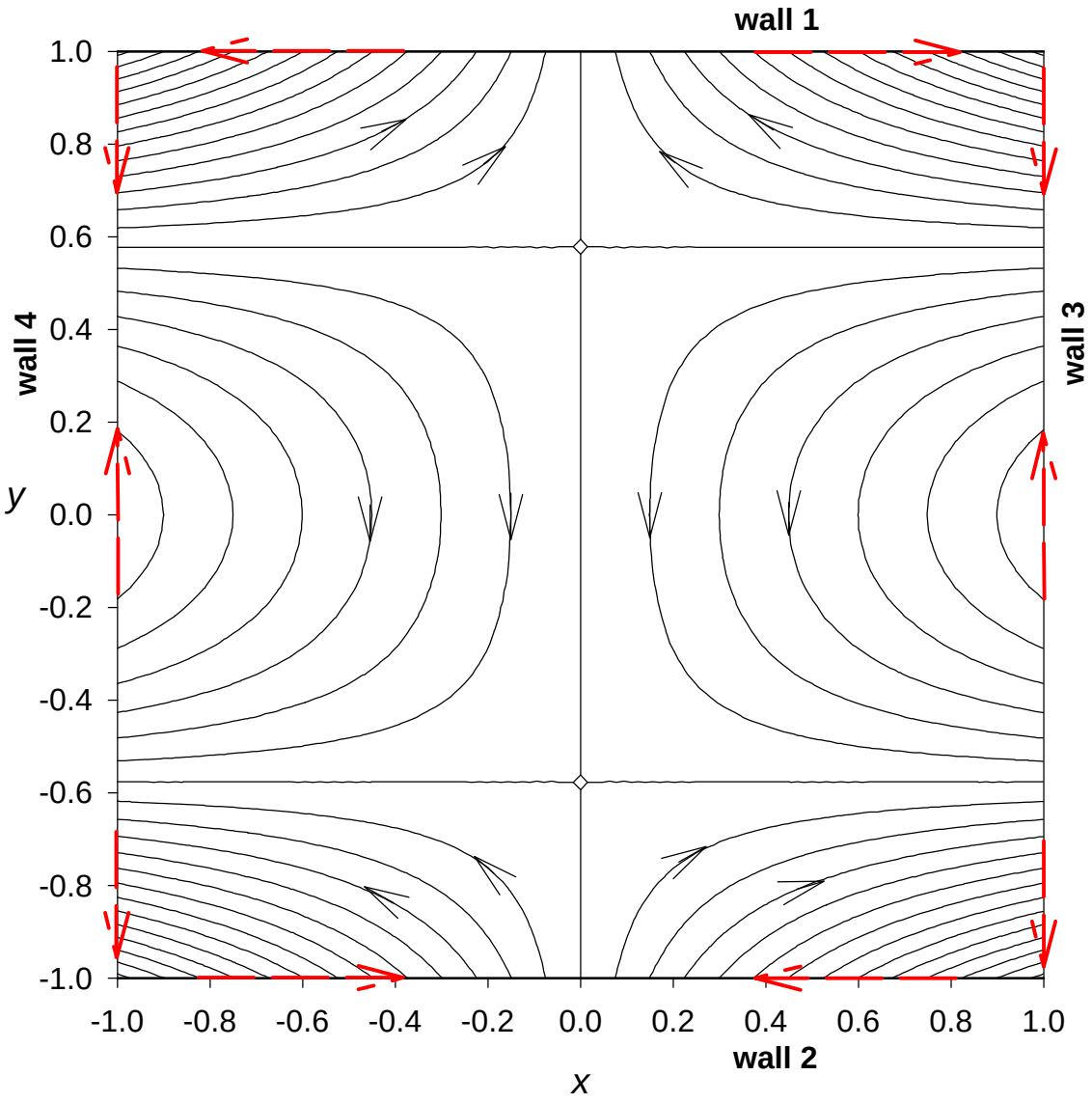

Fig. 4 Lines of core current for $T = xy$. All walls are perfectly conducting.

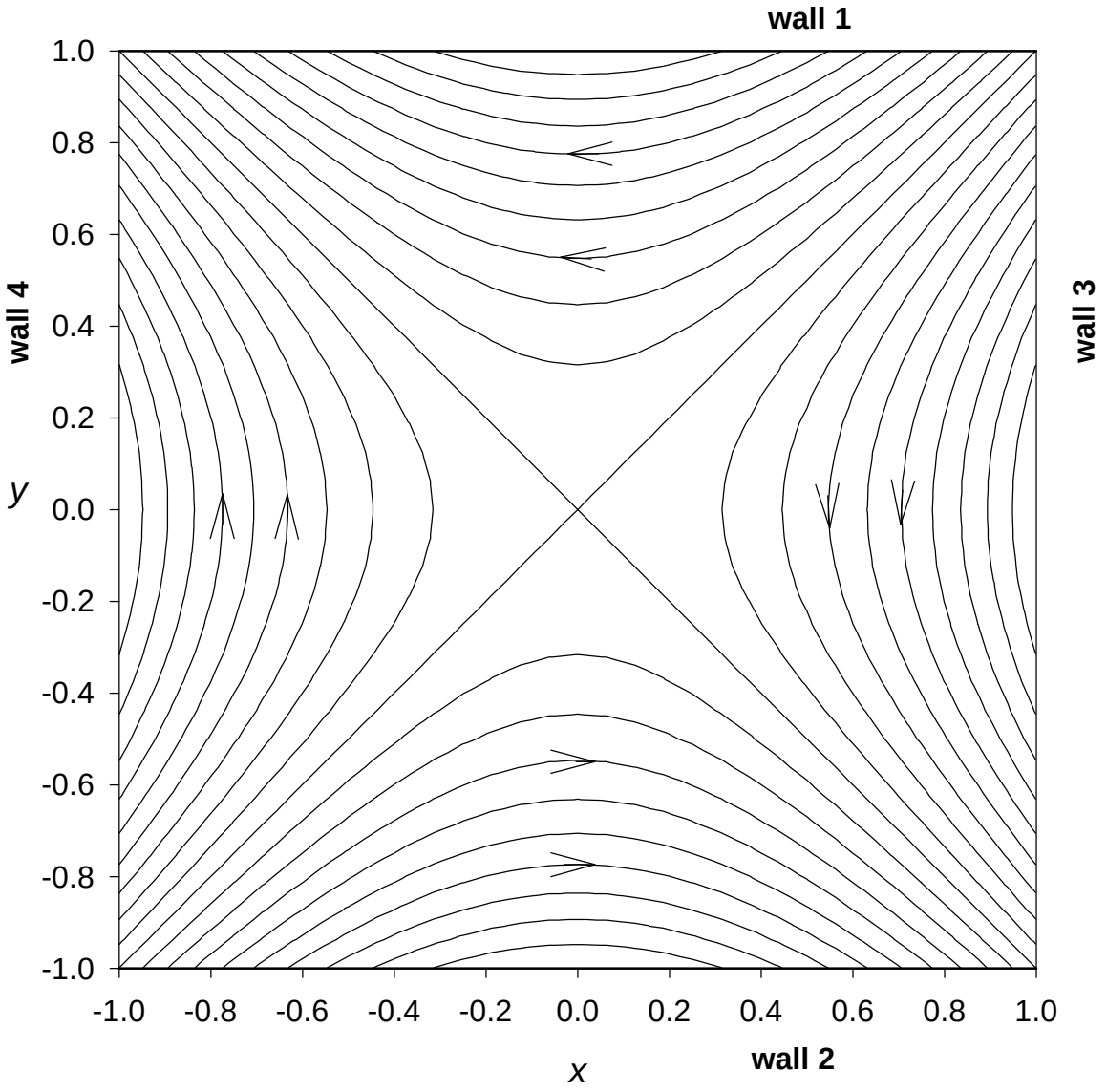

Fig. 5 Vector lines of local flow rate in layer *P5* for $T = xy$.

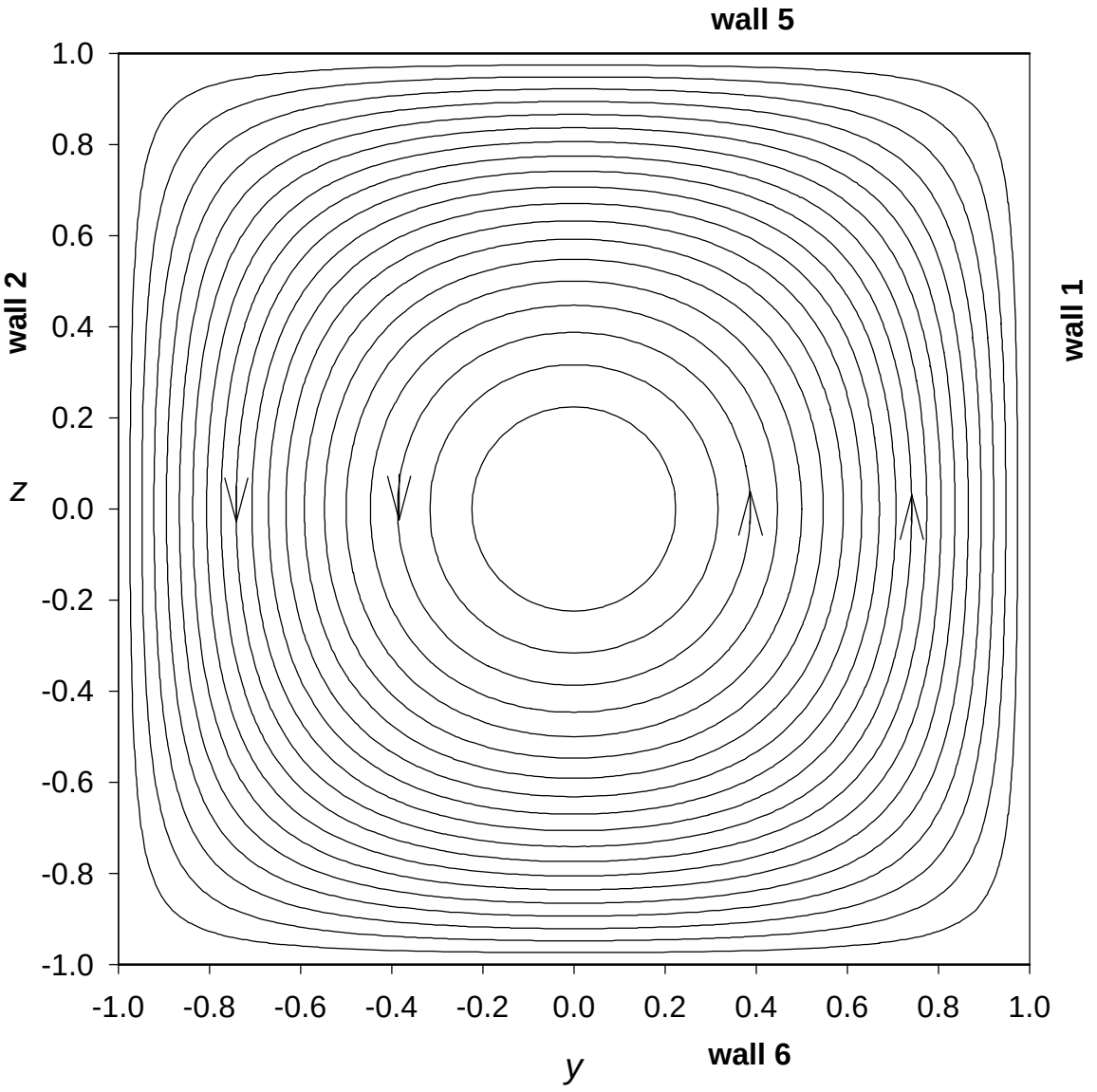

Fig. 6 Streamlines for $T = y(1-z^2)$. All walls are perfectly conducting.

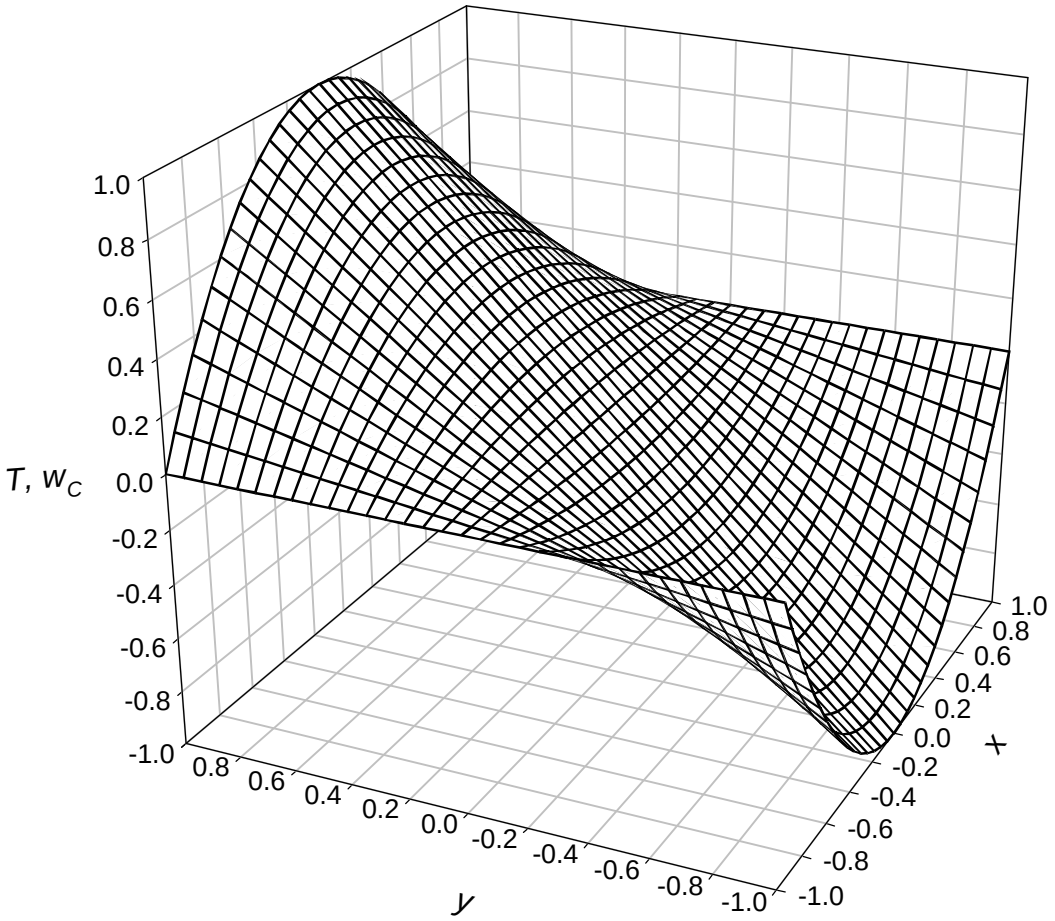

Fig. 7 Temperature $T = y(1-x^2)$ and vertical component of core velocity. Perfectly conducting walls 1 and 2.

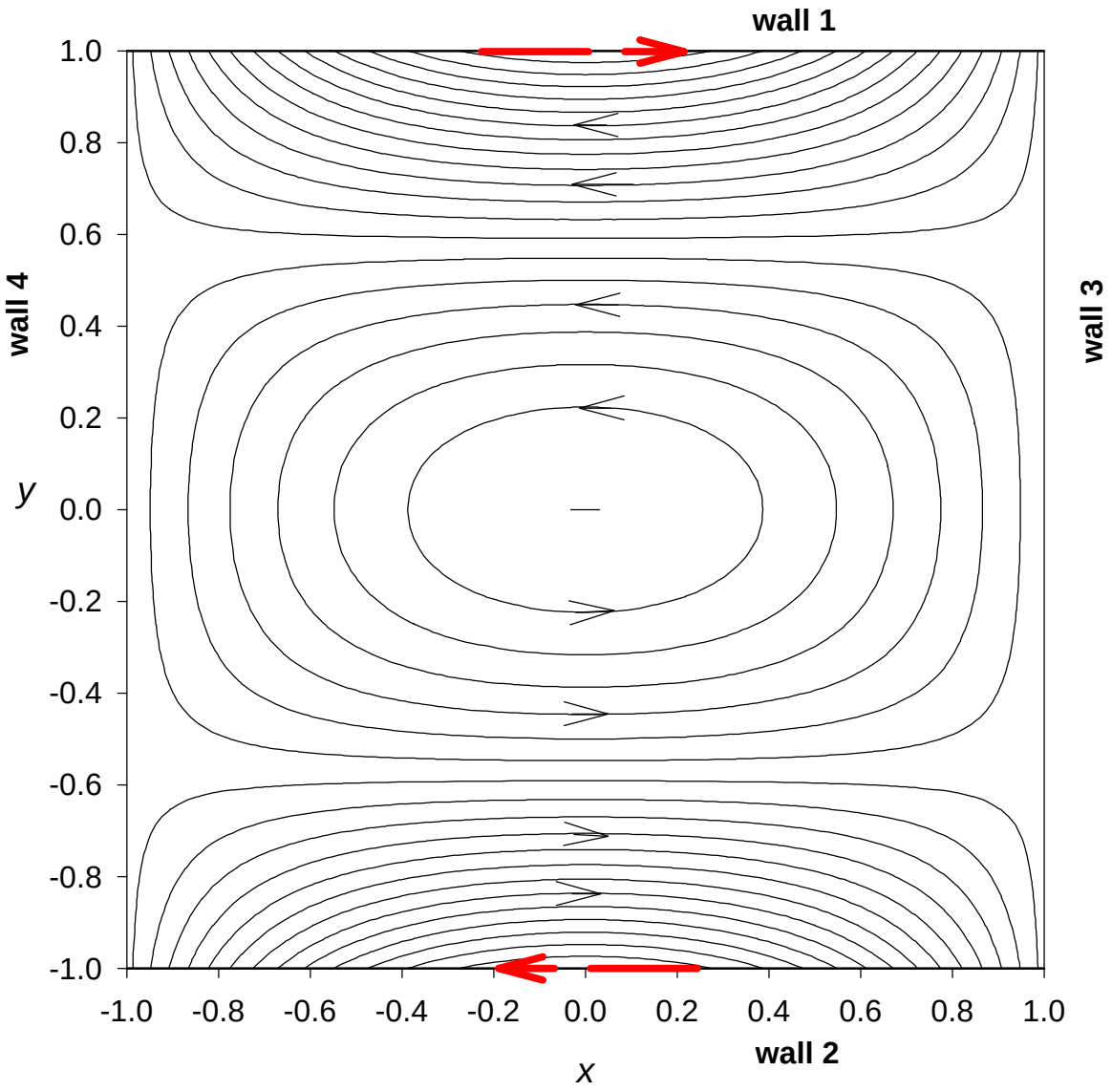

Fig. 8 Lines of core current for $T = y(1-x^2)$. Perfectly conducting walls 1 and 2. No current enters walls 3 or 4.

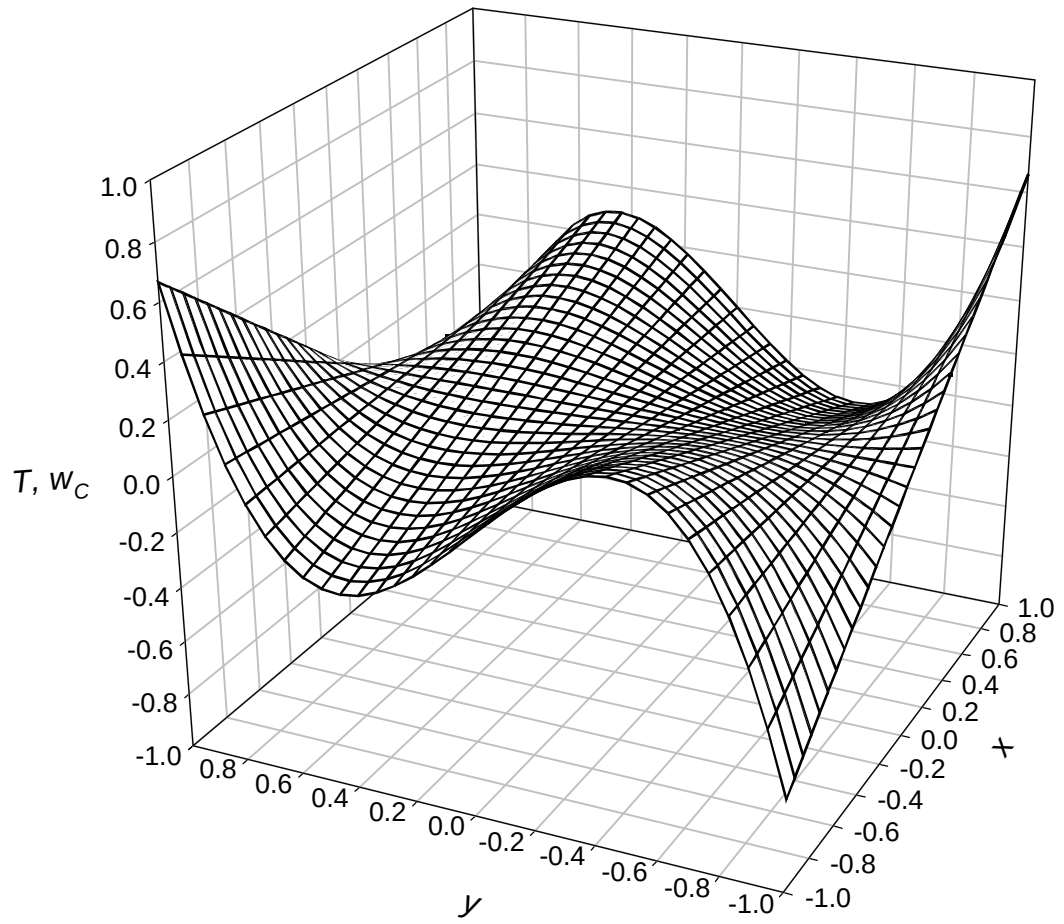

Fig. 9 Temperature $T = xy(1-5y^2/3)$ and vertical component of core velocity. Perfectly conducting walls 3-6.

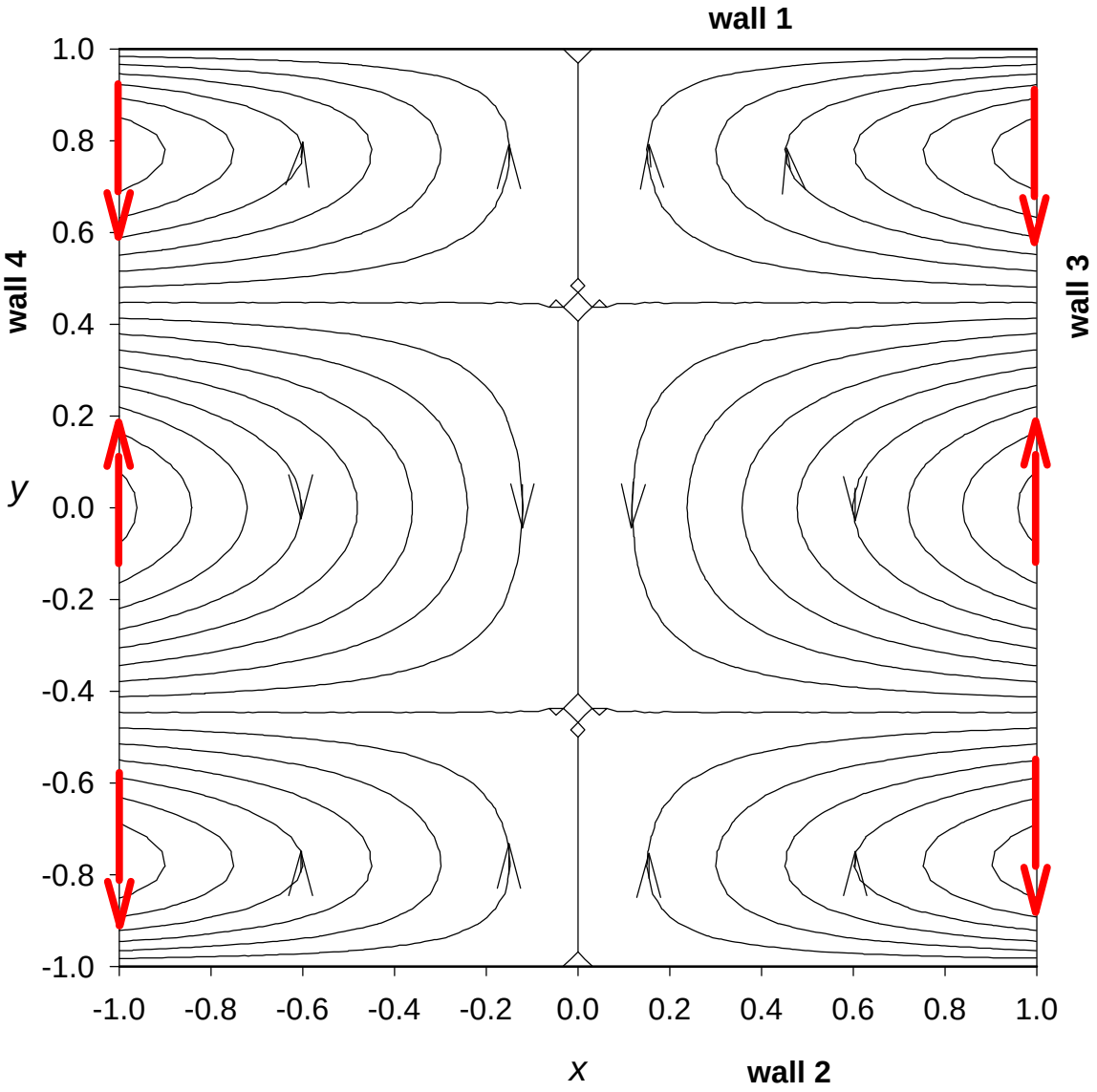

Fig. 10 Lines of core current for $T = xy(1-5y^2/3)$. Perfectly conducting walls 3-6. No core current enters walls 1 or 2.

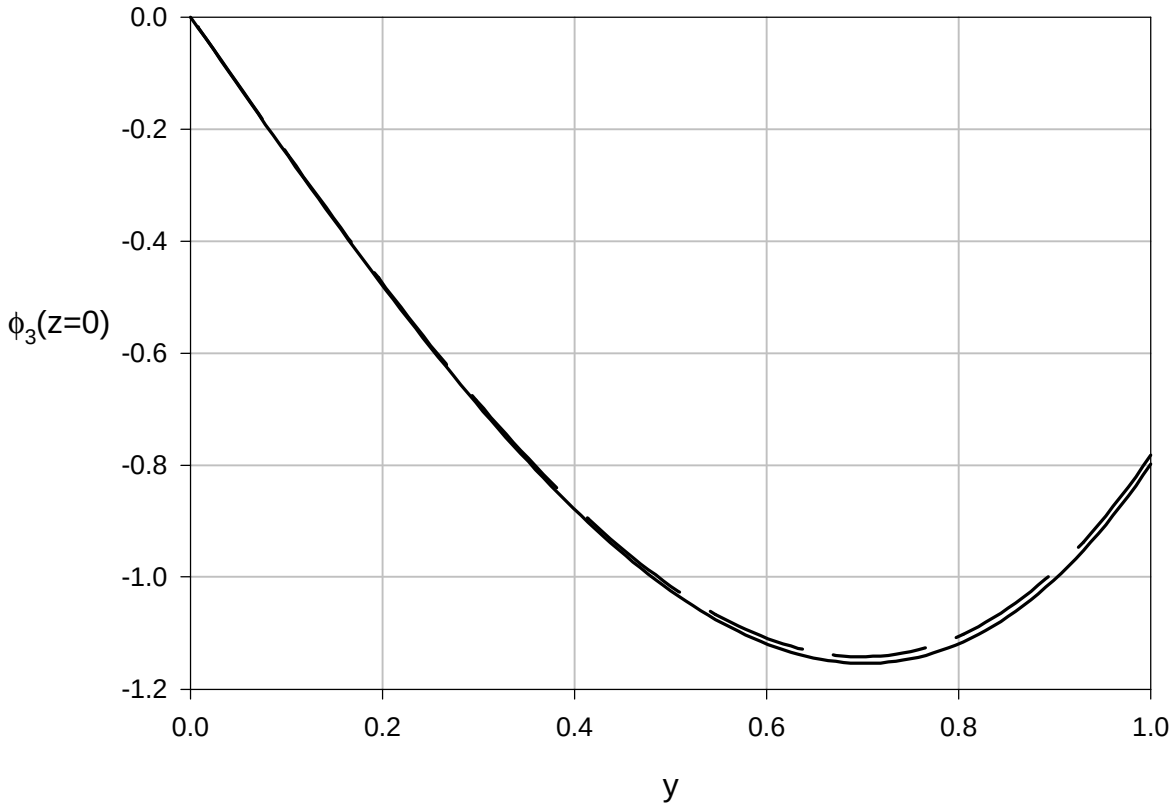

Fig. 11 Electric potential of wall 3 at z = 0 (broken line) and corresponding fully developed solution (solid line) for $T = y$, $l = 1$, $d = 5$, $c = 0.1$.

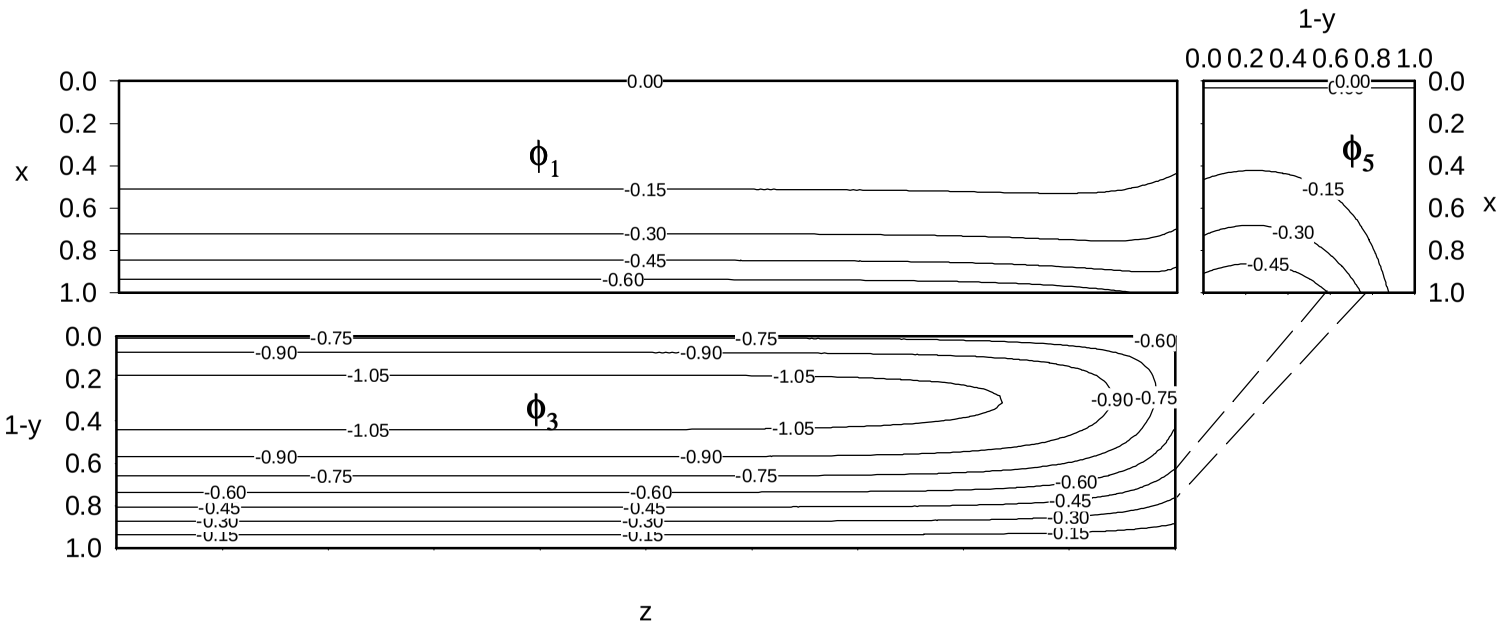

Fig. 12 Isolines of electric potentials of walls 1, 3, and 5 for $T = y$, $l = 1$, $d = 5$, $c = 0.1$. The wall currents are transverse to these isolines. Broken lines on the right show connection between isolines of ϕ_3 and ϕ_5.

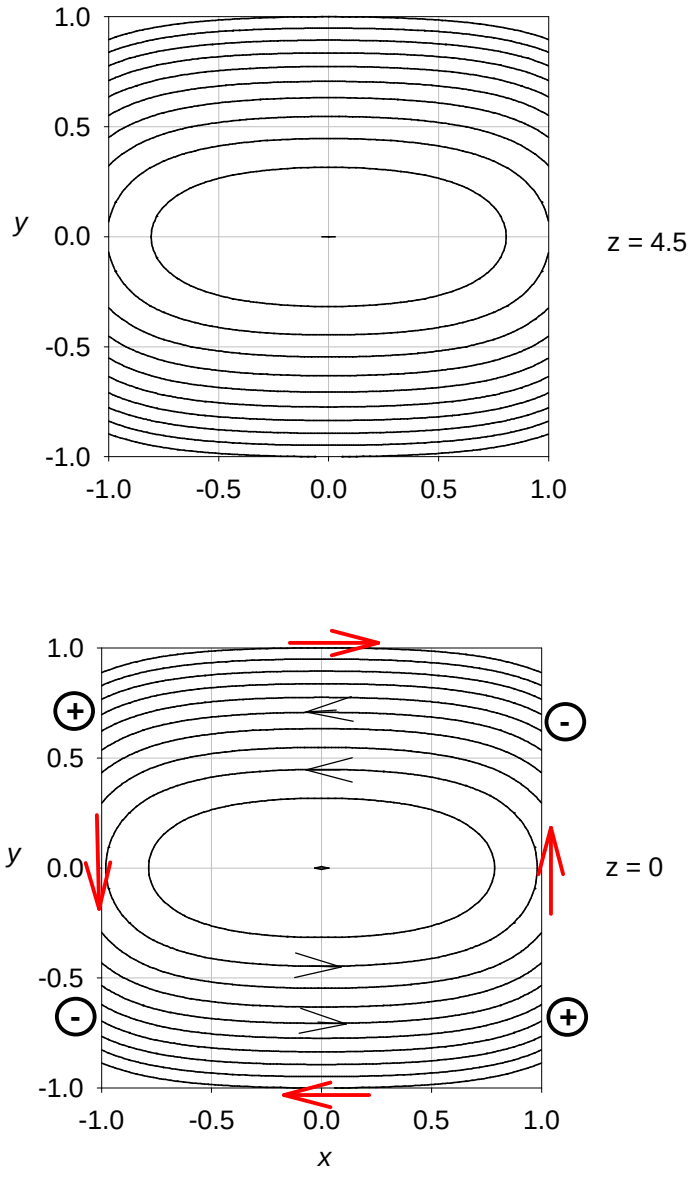

Fig. 13 Lines of core current in planes z = constant for *T* = *y*, *l* = 1, *d* = 5, *c* = 0.1. The approximate position of the minima and maxima of wall potential is shown with circles. The direction of wall current is shown with red arrows.

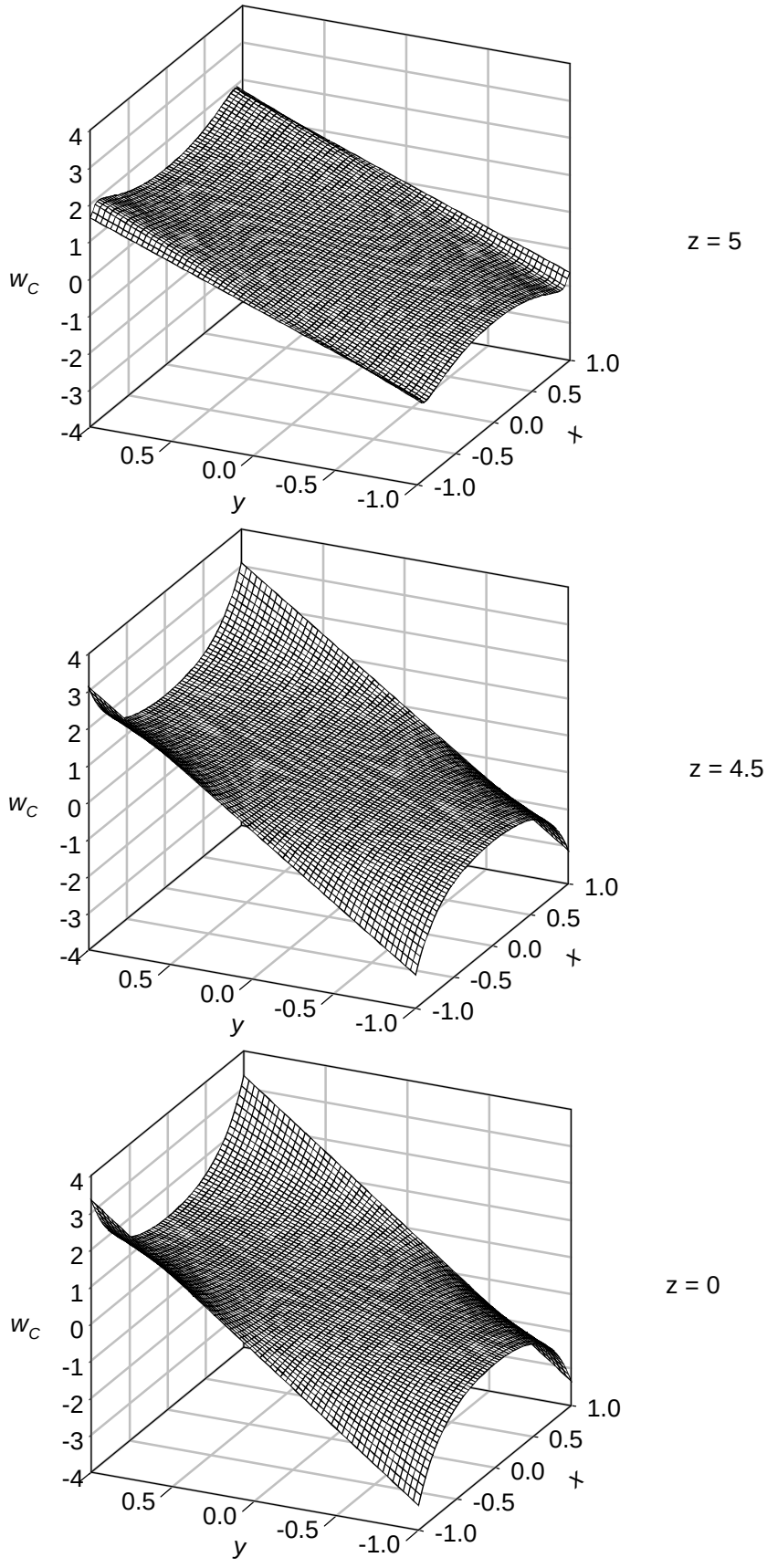

Fig. 14 Vertical component of core velocity for *T* = *y*, *l* = 1, *d* = 5, *c* = 0.1.

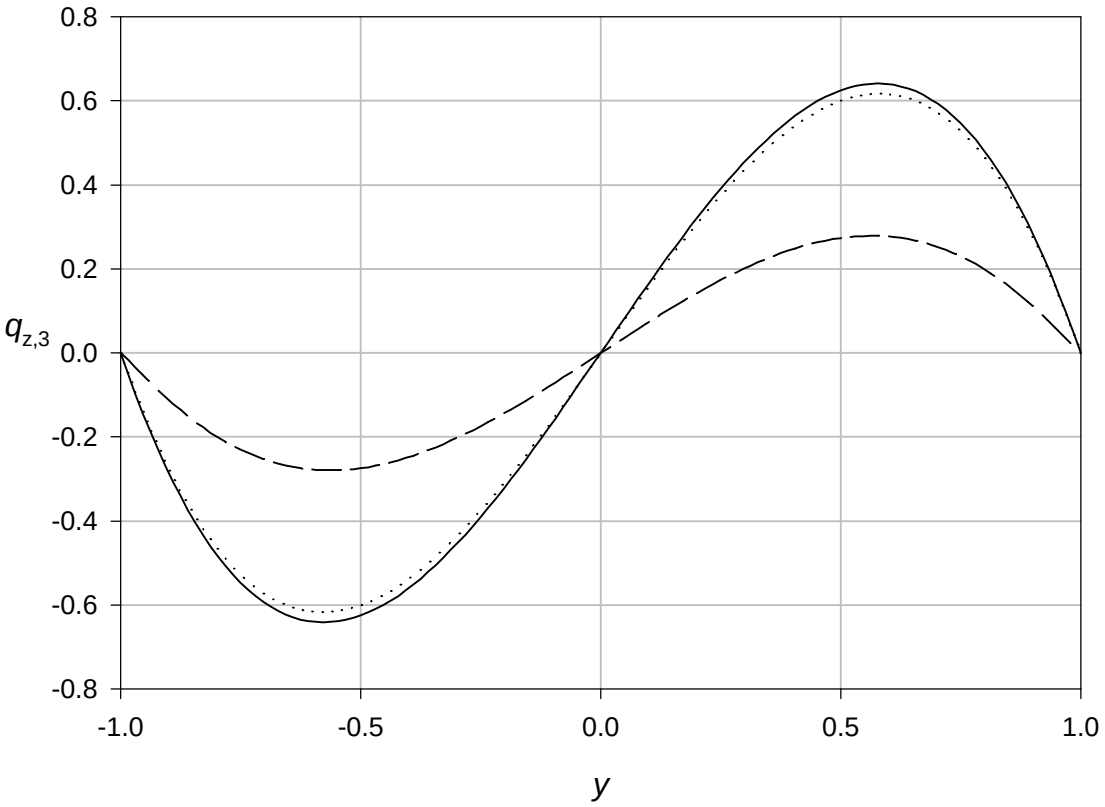

Fig. 15 z-component of the local flow rate in layer *P3* at $z = 0$ (solid line), $z = 4$ (dotted line) and $z = 5$ (broken line) for $T = y$, $c = 0.1$, $d = 5$, $l = 1$.

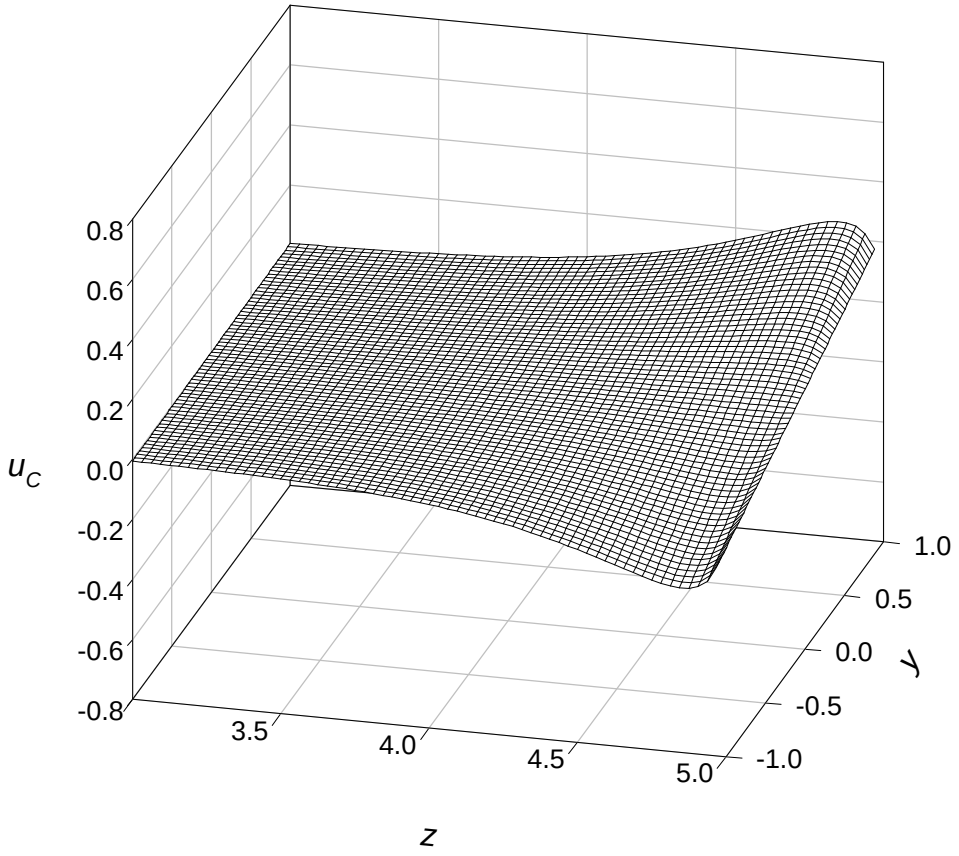

Fig. 16 *x*-component of core velocity at $x = l$ close to the top of the box for $T = y$, $l = 1$, $d = 5$, $c = 0.1$.

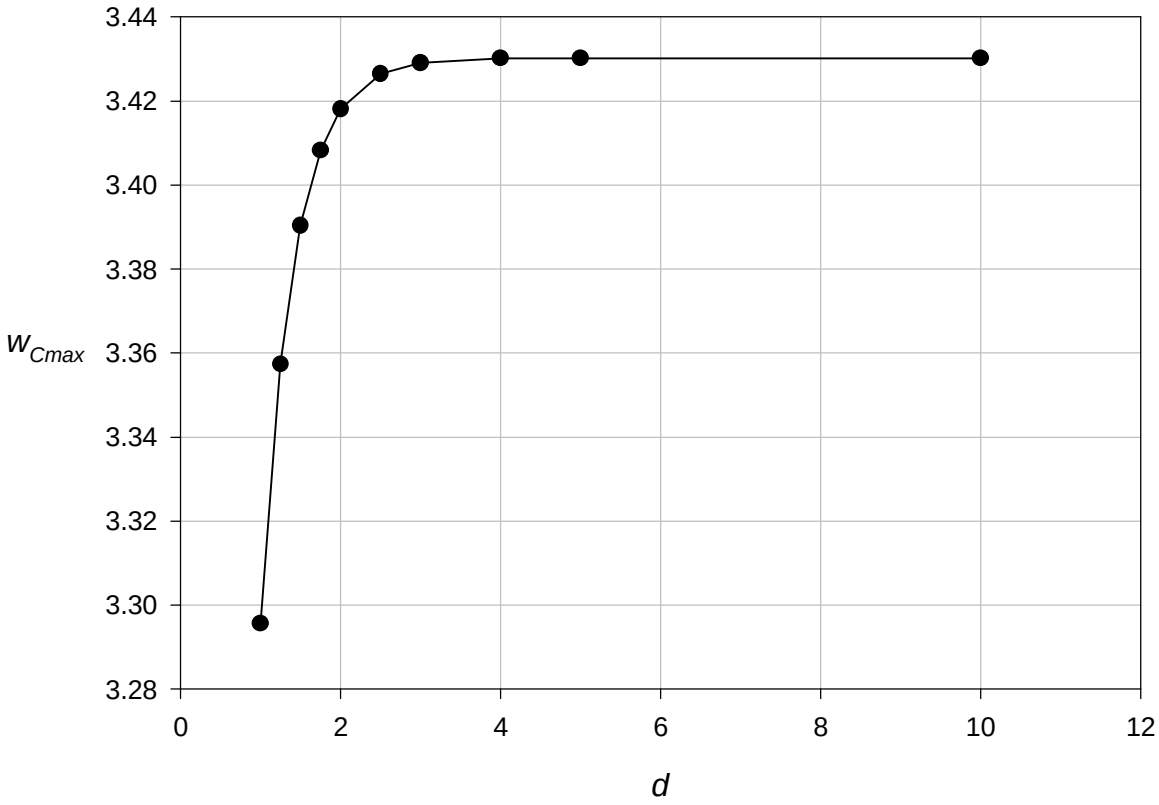

Fig. 17 Variation of the maximum of the vertical component of velocity at $z = 0$ with d for $T = y$, $l = 1$, $c = 0.1$.

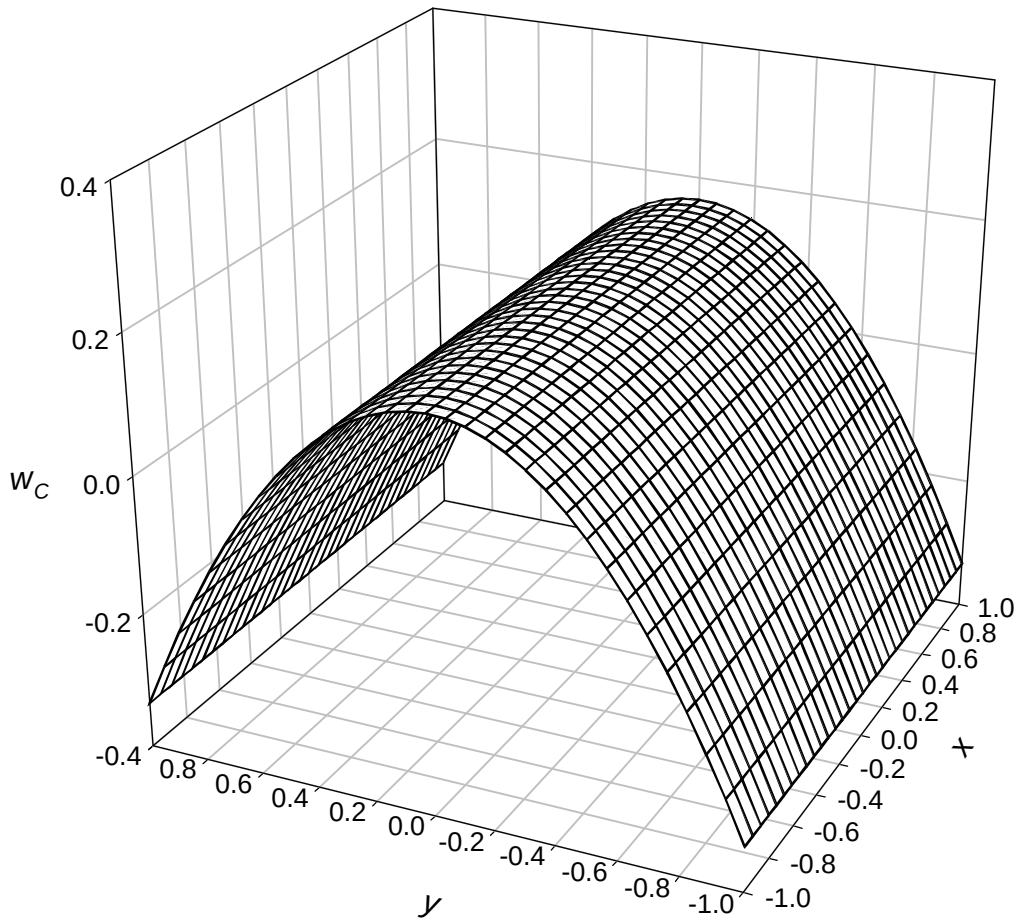

Fig. 18 Vertical component of core velocity for $T = (1-y^2)/2$.
All walls perfectly conducting.

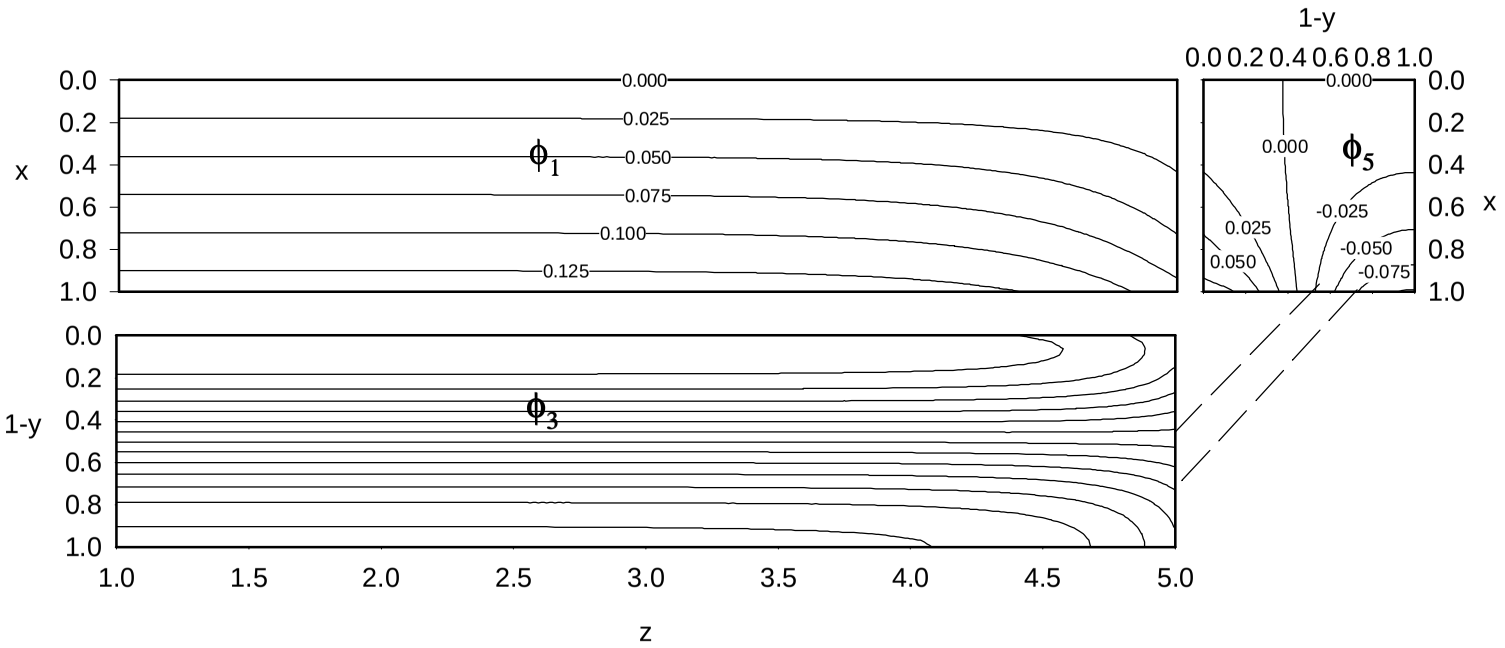

Fig. 19 Isolines of electric potentials of walls 1, 3, and 5 for $T = (1-y^2)/2$, $I = 1$, $d = 5$, $c = 0.1$. The wall currents are transverse to these isolines. Broken lines on the right show connection between isolines of ϕ_3 and ϕ_5.

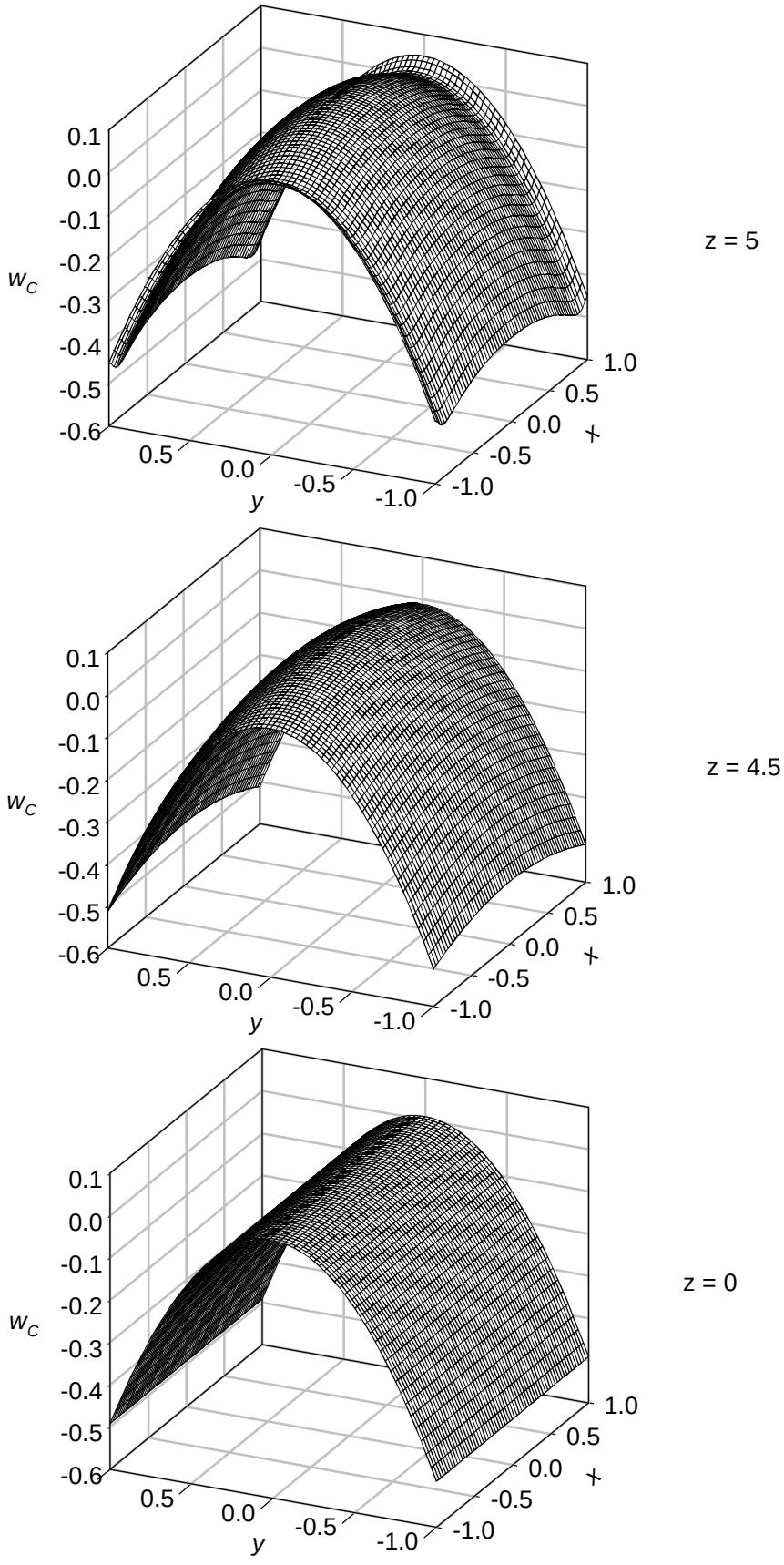

Fig. 20 Vertical component of core velocity for $T = (1-y^2)/2$, $l = 1$, $d = 5$, $c = 0.1$.

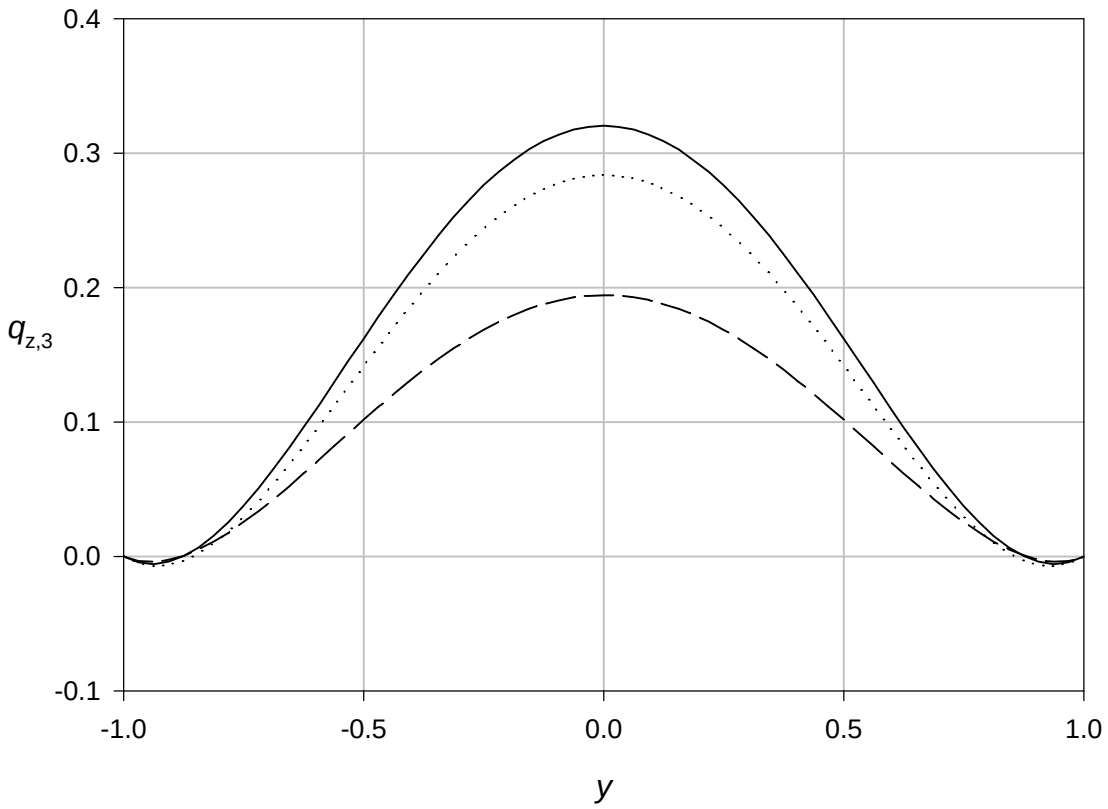

Fig. 21 z-component of the local flow rate in layer *P3* at $z = 0$ (solid line), $z = 4$ (dotted line) and $z = 5$ (broken line) for $T = (1-y^2)/2$, $c = 0.1$, $d = 5$, $l = 1$.

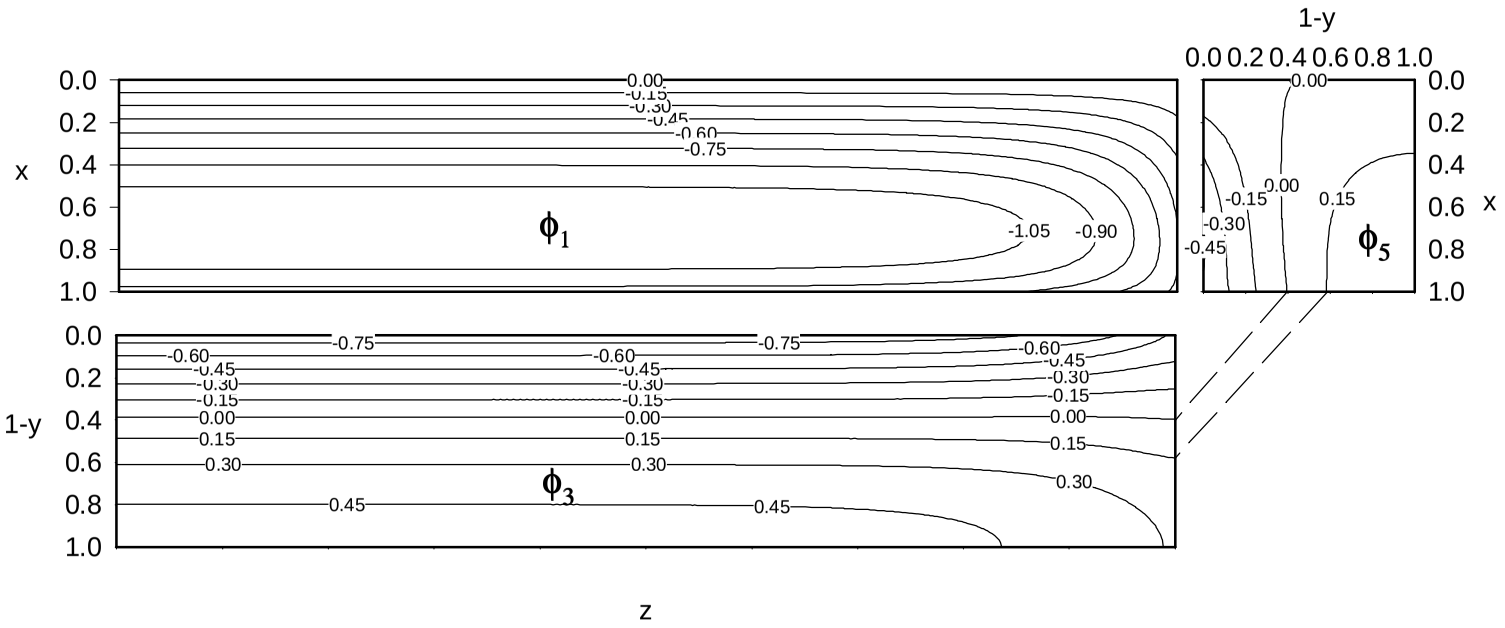

Fig. 22 Isolines of electric potentials of walls 1, 3, and 5 for $T = (1-x^2)/2$, $l = 1$, $d = 5$, $c = 0.1$. The wall currents are transverse to these isolines. Broken lines on the right show connection between isolines of ϕ_3 and ϕ_5.

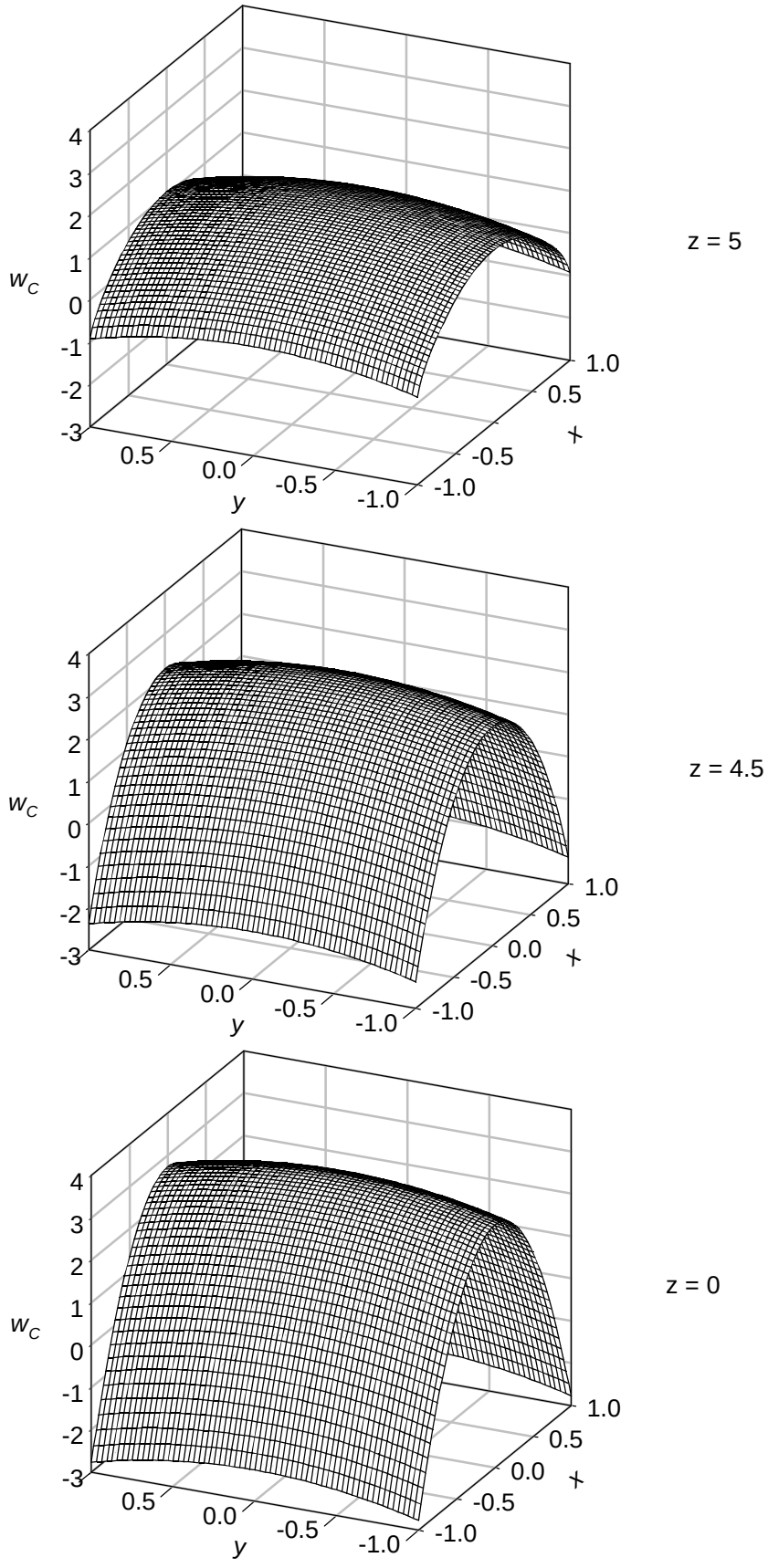

Fig. 23 Vertical component of core velocity for $T = (l^2-x^2)/2$, $l = 1$, $d = 5$, $c = 0.1$.

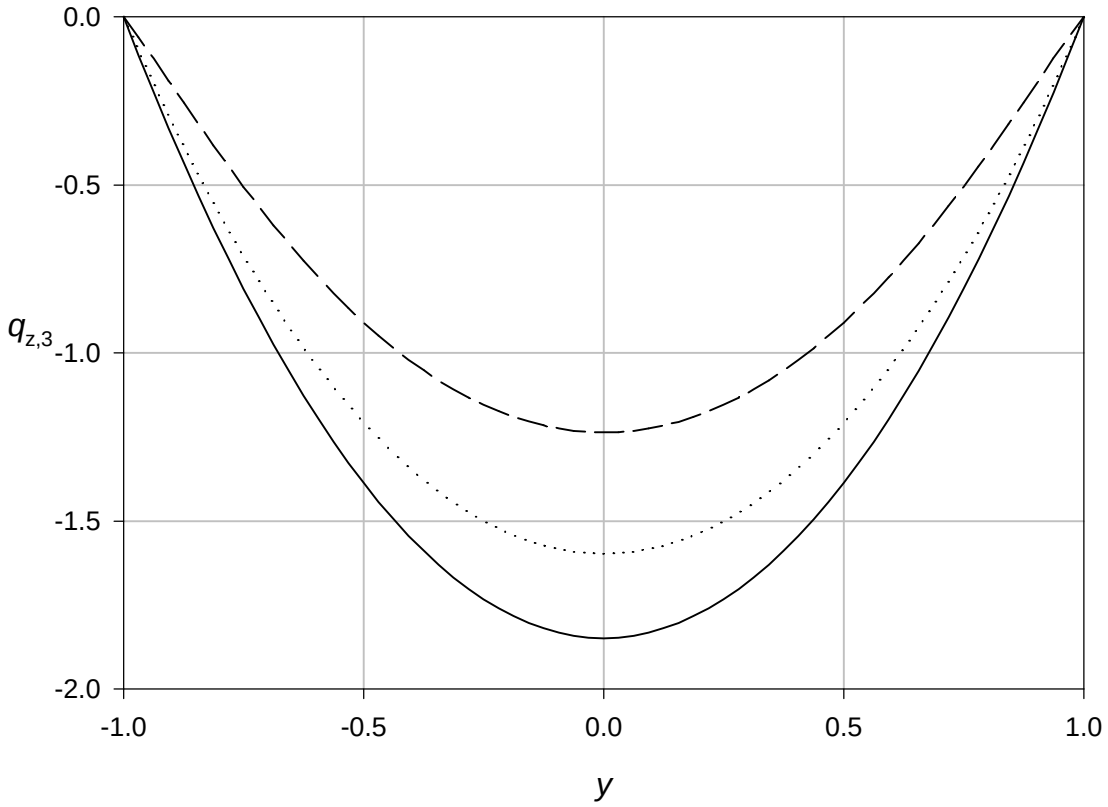

Fig. 24 z-component of the local flow rate in layer *P3* at $z = 0$ (solid line), $z = 4$ (dotted line) and $z = 5$ (broken line) for $T = (1-x^2)/2$, $c = 0.1$, $d = 5$, $l = 1$.

Fig. 25 Development of core pressure along the z-axis at x = 0 (solid line), and $x = l$ (dotted line) for $T = (1-x^2)/2$, $c = 0.1$, $d = 5$, $l = 1$.